Title

Response of shallow foundations in tire derived aggregate

Authors

Yarahuaman, AA
McCartney, JS

Publication Date

2024

DOI

10.1680/jgein.23.00147

Peer reviewed

RESPONSE OF SHALLOW FOUNDATIONS IN TIRE DERIVED AGGREGATE

By A.A. Yarahuaman, Ph.D. [1] **and J.S. McCartney, Ph.D., P.E., F.ASCE**[2]

ABSTRACT: This study investigates the quasi-static bearing stress-settlement response of shallow foundations in monolithic tire derived aggregate (TDA) layers having a total thickness of 3 m using a large-scale container and loading system. Tests were performed on footings having a range of widths, embedment depths, shapes, and loading inclinations. In tests where tilting was restricted, a clear bearing capacity was not observed for settlements up to 1.2B, where B is the footing width, but in tests where tilting was permitted bearing capacity was observed between settlements of 0.2B to 0.7B. Surface settlements indicate a dragdown response of the TDA adjacent to the footing extending out to more than 3B from the footing center, while settlement plates beneath the footing indicate a zone of influence of induced settlements of 14% at a depth of 4B. While bearing capacity theories for frictional geomaterials provided a reasonable prediction of the bearing capacity of footings in TDA for most tests, the corresponding settlements may be excessive for engineering applications. Accordingly, a correlation was developed between the theoretical bearing capacity and bearing stress at a settlement of 0.1B. A test with sustained loading indicates slight creep settlements with some stress dependency with magnitudes consistent with past studies.

KEYWORDS: Geosynthetics; Tire Derived Aggregate; Footings/Foundations; Bearing Capacity; Large-Scale Testing

[1] PhD Candidate, Department of Structural Engineering, University of California San Diego, 9500 Gilman Dr., La Jolla, CA 92093-0085; Email: ayarahua@ucsd.edu
[2] Professor, Department of Structural Engineering, University of California San Diego, La Jolla, CA 92093-0085; Email: mccartney@ucsd.edu

1. INTRODUCTION

The United States has experienced an exponential increase in the number of end-of-life waste tires (CalRecycle 2022). To avoid stockpiling or incineration, waste tires can be recycled and used for civil engineering projects in the form of tire-derived aggregate (TDA) as an alternative backfill material following ASTM D6270 (ASTM 2020). Multiple studies have been conducted to assess the feasibility of using TDA as a lightweight fill material in embankments or retaining walls (e.g., Drescher and Newcomb 1994; Hoppe 1994; Tweedie et al. 1998; Humphrey 2008a; Mills and McGinn 2010; Tandon et al. 2007; Meles et al. 2014; McCartney 2021), or as a bridging material for buried pipelines (Mahgoub and El Naggar 2020). TDA has good performance in these applications due to its similar or better shear strength compared to conventional fill soils (Humphrey et al. 1992, Bosscher et al. 1993; Hoppe 1998; Dickson et al. 2001; El Naggar et al. 2016; Ghaaowd et al. 2017). An advantage of using TDA as a backfill is that its unit weight ranges from 5-8 kN/m^3, which is about 33-50% of most granular backfill soils (Ghaaowd et al. 2017). TDA is more deformable than granular backfill soils and may experience limited creep under sustained load (Wartman et al. 2007; Humphrey 2008b; Adesokan et al. 2020; Yarahuaman and McCartney 2023), an issue that is accounted for in practice by overbuilding the TDA layer so that it reaches the desired elevation after surcharge loading (Humphrey 2008b). Due to its advantageous dynamic properties including low shear modulus, high damping, and high displacement at peak shear strength (e.g., Senetakis et al. 2012; Ghaoowd et al. 2017; McCartney et al. 2017), TDA can be used to decrease seismic induced lateral stresses on retaining walls (Ahn and Cheng 2014) or to provide a compliant foundation for seismic isolation of buildings or bridges (Tsang et al. 2020).

The two main categories of TDA defined by ASTM D6270 are Type A TDA, with particle sizes ranging from 75-100 mm, and Type B TDA, with particle sizes ranging from 150-300 mm. Type B TDA is more cost-effective because it requires less processing than Type A TDA and has lower risk of self-heating due to the smaller amount of exposed steel wire in the larger particles. Accordingly, ASTM D6270 prescribes that Type B TDA layers can have a thickness up to 300 mm while Type A TDA layers are limited to a thickness of 100 mm. Although Type B TDA is the main type of TDA recommended for use in practice, only a few studies with large-scale testing capabilities have investigated its internal shearing properties (Ghaaowd et al. 2017; Fox et al. 2020), interface shearing properties (Ghaaowd et al. 2017, 2020), cyclic shearing properties (McCartney et al. 2017), and compression response (Meles et al. 2014; Adesokan et al. 2020; Yarahuaman and McCartney 2023). Accordingly, there is a need to investigate the use of the material properties from these studies to predict the response of geotechnical systems involving Type B TDA. Many studies have investigated the behavior of tire shreds mixed with soil, as this strategy leads mitigates risks of exothermic reactions and leads to satisfactory mechanical properties. However, mixing tire shreds with soil is not a recommended reuse option for waste tires because of the additional labor and cost required for mixing, the increase in the unit weight of the backfill due to the addition of soil, and the fact that it does not maximize the reuse of TDA. Using monolithic layers of TDA following guidance from ASTM 6270 permits the maximum reuse of waste tires and fully takes advantage of the lightweight characteristics of TDA.

This study focuses on measurement of the quasi-static bearing stress-settlement response of large-scale concrete footings embedded in a monolithic layer of Type B TDA with the maximum thickness permitted by ASTM D6270 of 3 m. The bearing capacity is important for designing shallow foundations for signposts, guardrails, or thrust blocks for water pipelines that may be installed in a TDA backfill layer in an embankment or retaining wall. The stress-settlement response and stress distribution in TDA are also important when designing the thickness of bridging materials for buried pipelines (Mahgoub and El Naggar 2020). The bearing capacity is also a critical quantity needed to predict the response of rocking footings, which are foundations designed to yield during earthquake shaking (Gajan and Kutter 2008; Deng and Kutter 2012). Rocking footings in TDA may be a new way to incorporate TDA into geotechnical seismic isolation (GSI) systems for buildings or transportation infrastructure (Tsang et al. 2012, 2020). As Tsang et al. (2012, 2020) studied rocking footings in rubber-soil mixtures, there is still a need to understand the bearing capacity of foundations in monolithic Type B TDA layers as part of the design of GSI systems which have recently been studied by Yarahuaman and McCartney (2024).

While some studies have investigated the bearing response of footings in tire shreds mixed with soil (e.g., Arefnia et al. 2021; Chenari et al. 2017), few have studied the bearing response of footings in monolithic layers of TDA. There have been a few studies focused on the bearing capacities of footings on granular soil layers overlying TDA. Mahgoub and El Naggar (2020) studied the performance of rigid footings resting on a surface of conventional soil backfill soil overlying a TDA layer and considered three full-scale field tests with different TDA layer thicknesses. A 3D finite element numerical model was developed using the results of the field tests to evaluate the failure mechanism of shallow foundations overlaying a layer of TDA, and the TDA layer helped improve the stress transfer from the footing by reducing its zone of influence. Mahgoub and El Naggar (2022) developed a simplified design method to estimate the ultimate bearing capacity of shallow foundations built on top of TDA while considering the overlying granular layer thickness, TDA layer thickness, footing width, footing shape, footing depth, and allowable settlement. They noted that because TDA is highly compressible, the design of footings in TDA should be based on the bearing stress at an allowable settlement level. This requires measurement of the bearing stress-settlement curve for footings in TDA.

The objective of the testing program in this study is to investigate the effects of footing dimensions, footing embedment, footing shape, and load inclination angle on the stress-settlement response of shallow footings in Type B TDA using quasi-static loading tests. A goal is to measure the bearing capacity based on ultimate load conditions and settlement serviceability conditions and compare these measured values with predictions from bearing capacity theories for granular soils in the literature (e.g., Hansen 1970) using shear strength parameters for Type B TDA obtained from the large-scale direct shear tests of Ghaaowd et al. (2017).

2. EXPERIMENTAL SETUP AND TESTING PROGRAM

A large rectangular container was constructed for the testing program in this study in the South Powell Laboratory at UC San Diego with the goal of performing loading tests on footings within a Type B TDA layer having the maximum thickness permitted in ASTM D6270 of 3 m. The container employed the strong floor and strong wall of the laboratory as the base and one side of the container, respectively, and used pre-cast concrete panels from the soil confinement box developed by Fox et al. (2015) for the large high performance outdoor shaking table at UCSD to form the other sides of the container. The concrete panels were post-tensioned to the strong floor and strong wall to provide a rigid boundary suitable to replicate plane strain conditions. Schematics of the container are shown in Figures 1(a), 1(b), and 1(c). An “A” frame was connected to the strong wall to provide a reaction support for loading actuators used to apply vertical or inclined loads to the footing, as shown in Figure 1(d).

After assembly of the container, the sides were covered with two layers of visqeen sheeting to minimize side-wall friction. Type B TDA was placed into the container in 300 mm-thick lifts as shown in Figure 2(a). The particle size distribution and engineering properties of the Type B TDA used in this study are summarized by Ghaaowd et al. (2017). The TDA was compacted using a skid-steer loader weighing approximately 22.2 kN, which was lifted into the container using the overhead crane as shown in Figures 2(b) and 2(c). Each layer received 5 round-trip passes of the loader and was observed to visibly densify with reference to elevation marks on the sides of the container. The TDA particles tend to align horizontally and form interlocking connections after compaction. Embedded settlement plates were placed near the edges of the container to minimize interference with the compaction process as shown in Figure 2(c).

Schematics of the four concrete footings investigated in the testing program are shown in Figure 3. A precast strip footing having the same length as the container width and a width B and depth D of 0.46 m shown in Figure 3(a) was used as the baseline footing for the testing program. Vertical connectors were cast into the top of the concrete footing to accommodate the connection of a vertically oriented actuator. Further, additional connectors were cast into two bevels on the top surface to accommodate connections to an inclined actuator having angles from vertical of 30 or 60°. The footing also has four 100 mm-diameter through holes near the edges to accommodate tell-tales for settlement plates embedded in the TDA layer. A second precast strip footing having a similar design to the baseline footing but with a greater width B and depth D of 0.91 m is shown in Figure 3(b). Two cast-in-place cylindrical footings having diameters B of 0.46 and 0.30 m shown in Figures 3(c) and 3(d) were evaluated to assess the impact of footing shape, and to represent the most-likely footing type for guard-rails or signposts installed into a TDA retaining wall. The cast-in-place footings were fabricated by placing a cardboard tube form onto the surface of a TDA layer, excavating the TDA from the center of the tube to the desired embedment depth of 0.3 m, then placing concrete into the form to create the footing. The concrete had sufficiently low slump that it did not flow into the TDA, and the final diameter of the concrete evaluated after extracting the footing at the end of testing was within the thickness of a TDA particle from the interior diameter of the tube form. The foundations were cured for 28 days in-situ before testing. This approach led to a rough concrete surface that was bonded to individual TDA pieces and was intended to represent placement conditions of this type of footing in the field.

Details of the TDA layers and footings in the testing program are summarized in Table 1. Tests QT-01 through QT-03 were performed on the baseline strip footing with vertical loading, Test QT-04 was performed on the large strip footing with vertical loading, Tests QT-05 and QT-06 were performed on the cylindrical footings with vertical loading, and tests QT-07 and QT-08 were performed on the baseline strip footing with inclined loading. During the sequence of the testing program, all the TDA was not fully removed from the container after each test due to the significant volume of TDA. Instead, the TDA within 2B of the footing base was excavated and recompacted. While this process undoubtedly led to variability in the characteristics and properties of the TDA layers tested, the volume of TDA removed and replaced was carefully monitored to track the average TDA layer unit weight as summarized in Table 1. The average friction angle of the Type B TDA corresponding to the average initial vertical stress at mid-height of the TDA layer calculated using these average unit weight values was estimated using the nonlinear failure envelope of Ghaaowd et al. (2017).

The experimental protocol for each test is summarized in Table 2. The testing program evolved for several reasons. Test QT-01 was performed on the baseline footing with no embedment with a single actuator in load control conditions, shown in Figure 4(a). Loading was paused in this test at three loads to study creep deformations and the test was stopped near the capacity of the actuator of 222 kN without reaching a clear bearing capacity failure. It was hypothesized that the swivel at the actuator connection did not sufficiently permit tilting in Test QT-01. Test QT-02 was performed on the baseline footing but with two actuators in displacement control mode. While there was a swivel connection between each actuator and the footing, no tilting occurred as both actuators advanced at the same displacement rate. Test QT-02 was stopped at the maximum stroke of the actuators and a clear bearing capacity was also not observed. Test QT-03 shown in Figure 4(b) had the same confirmation as Test QT-02 but the actuators were operated in load control and tilting failure was observed to occur. Test QT-04 was performed on the larger strip footing in embedded conditions with a similar actuator configuration to Test QT-03 operated in load control as shown in Figure 4(c), and tilting failure was observed. Test QT-05 shown in Figure 4(d) and Test QT-06 were performed with a single actuator due to their smaller size, and tilting failure occurred in both tests. Tests QT-07 and QT-08 shown in Figures 4(e) and 4(f), respectively, were performed with a single inclined actuator connected directly to the strong wall, and tilting failure was observed in both tests. In all tests, the load and unloading rates summarized in Table 2 were slow enough to avoid inertial effects.

Each test included a variety of instruments to measure the bearing stress-settlement response of the footing along with the internal and surficial deformation response of the TDA. A typical instrumentation plan for Test QT-03 is shown in Figure 5. The layout in the other tests is similar. Three earth pressure cells were placed at the base of the container to measure the self-weight stresses and stresses induced through the TDA layer. Eight settlement plates were placed on the TDA surface along with four on the edges of the footing. Three settlement plates were embedded in the TDA layer outside of the footing, and three were embedded in the TDA layer under the footing. The embedded settlement plates were connected to potentiometers at the surface using tell-tales consisting of a threaded rod within a PVC pipe. Two potentiometers were attached to metal angles extending vertically from the footing to track the tilting angle of the footing. The force and displacement of each actuator was also monitored. An accelerometer was placed on the top of the footing for vibration tests, which is the scope of another paper.

3. RESULTS

The time series from the instrumentation in Test QT-03 are shown in Figure 6. While each of the tests is slightly different, the time series from Test QT-03 are useful in understanding typical measurements during the tests. The variation in the bearing stress is shown in Figure 6(a), with the initial stress at time zero associated with the self-weight of the footing. The stress increased at a linear rate in this load-controlled test. The average stress at the base of the TDA layer from the earth pressure cells is also shown in Figure 6(a), which shows a smaller increase than the bearing stress indicating that stresses are distributed through the TDA layer in a similar manner to footings on soils. The footing was rapidly unloaded after tilting was detected in the footing edge settlements shown in Figure 6(b). The surface settlements of the TDA are also shown in Figure 6(b), and monotonic increases in surface settlement at different distances from the footing center are observed. The distances from the footing center are positive in the north direction, and the footing edge settlement measurements are at ±0.2 m from the footing center. While some of the footing settlements were permanent unloading, most of the TDA surface settlements were recoverable except next to the footing. The tilt angle from potentiometers P05 and P06 in Figure 5 is shown in Figure 6(c) and indicates that tilting occurred rapidly up to 15 degrees when approaching the ultimate bearing stress of 238 kPa. During unloading, the footing tilted back in the other direction. The subsurface settlements of the TDA beneath the footing are shown in Figure 6(d), which indicates that there is a zone of influence extending to nearly 2 m from the surface of the TDA layer, which is permanent after the footing is unloaded. The subsurface settlements of the TDA outside of the footing area shown in Figure 6(e) indicate that settlements are induced by a stress distribution effect, with a magnitude that decreases with distance from the footing center.

The bearing stress versus footing settlement normalized by the width of the footing is shown Figure 7 for the six tests involving vertical loading. The stress-settlement curve for Test QT-01 shown in Figure 7(a) was performed in load control conditions where tilting was restricted up to a stress of nearly 200 kPa, after which the footing was unloaded then reloaded back to 240 kPa. Creep settlement was characterized during three periods at constant stress values as denoted by the vertical shifts in the curve. The shape of the curve is relatively linear during loading but is nonlinear during unloading. While the footing was able to reach relatively large bearing stresses, a normalized settlement of 1.2B or approximately 0.55 m was required to reach this bearing stress. The bearing stress-settlement curve for this test shows a hardening response with continued loading typical of a punching shear failure mechanism. To characterize the footing bearing response at the serviceability limit state, the bearing stress at a settlement of 0.1B is labeled in Figure 7(a). The bearing stress-settlement curve for Test QT-02 is shown in Figure 7(b). This test on the embedded footing was performed in displacement control conditions where tilting was restricted. Due to the embedment, higher bearing stresses of nearly 500 kPa were reached at a normalized settlement of 1.2B, but similar to Test QT-01, no clear failure was observed. Test QT-03 was essentially the same as test QT-02 but with load-controlled conditions and no tilting restriction so the average settlement differed from the settlements measured on the north and south sides of the footing. While the footing experienced tilting failure at a bearing stress of 238 kPa, the bearing stress at a normalized settlement of 0.1B of 42 kPa was nearly the same as the value of 44 kPa in Test QT-02. In Test QT-04, tilting failure occurred at a relatively low bearing stress of 153 kPa. Despite the premature tilting failure, this larger footing showed a stiffer response with a bearing stress at a normalized settlement of 0.1B of 90 kPa. The tilting failure in this test may have been due to a weaker pocket of TDA under one of the corners, which emphasizes the importance of careful compaction in TDA. The stress-settlement curves of the two cylindrical footings in Figures 7(e) and 7(f) indicate tilting failure with a larger ultimate bearing capacity for the footing with a large diameter. Overall, the results in Figure 7 indicate that Type B TDA shows a punching shear failure mode where failure will occur due to excess tilting for the case where tilting is not restricted. Vesic (1973) observed that footings in compressible soil layers typically experience punching shear failure rather than general shear failure or local shear failure, so this observation can be attributed as well to footings in compressible TDA layers. The punching failure mechanism is further supported by the lack of surface bulging observed in the TDA adjacent to the footing.

As noted in the time-series in Figure 6, the TDA around the footings can deform significantly during application of large bearing stresses. As an example, profile plots of the TDA deformations during Test QT-03 are shown in Figure 8, which are similar to the observations from the tests on the other vertically-loaded footings. The TDA surface consistently showed a drag-down response during loading as shown in Figure 8(a), where the footing penetrated into the TDA and the TDA up to a normalized distance of 3B also settled downward. During unloading, permanent settlement troughs were noted in the TDA, as shown in Figure 8(b). Below the footing, the TDA was also observed to compress up to depths of more than 4B from the TDA surface as shown in Figure 8(c). The settlement at a depth of 4B from the TDA surface was 14% of that induced by the footing loading. While this is still a large settlement compared to soils, there is a significant reduction in deformation with depth due to the compressibility of the TDA. During unloading, a permanent settlement with depth is also noted as shown in Figure 8(d), similar to the surface settlements. Profiles of the settlements of the TDA at a depth of 1B from the TDA surface in Figure 8(e) indicates that TDA subsurface settlements followed a similar trend with distance from the footing center as the TDA surface settlements but with smaller magnitudes. Permanent subsurface settlements were also observed after unloading as shown in Figure 8(f).

Interpretation of the inclined loading tests is more complex than the vertical loading tests as the actuator displacement is in the direction of the footing load, while the vertical settlements of the footing corners permit understanding of the tilt of the footing. In the test on the footing with an actuator inclined 30 degrees from vertical, the actuator displacement followed that of the north edge settlement further from the strong wall as shown in Figure 9(a), which indicates overturning during load application. In the test on the footing with an actuator inclined 60 degrees from vertical the actuator settlement differed from the settlements of the footing edges as the south edge tilted upwards and the north edge tilted downwards as shown in Figure 9(b). The stress-settlement curves were decomposed into vertical and horizontal components for comparison with the other tests. The test with an actuator inclined 30 degrees from vertical had a smaller horizontal stress component in Figure 9(c), while the test with an actuator inclined 30 degrees from vertical had a greater horizontal stress component, as shown in Figure 9(d). The ultimate bearing capacity for these footings were determined from the vertical stress-displacement components. The TDA surface in the test with an actuator inclined 30 degrees from vertical in Figure 9(e) showed a settlement profile similar to the vertical loading tests, but with a smaller zone of influence of less than 2B. The TDA in the test with an actuator inclined 60 degrees from vertical in Figure 9(f) was the only test to show a slight heave at a normalized distance of 1.75B from the footing center, as the large horizontal stresses induced in the TDA likely started to induce a passive wedge formation.

4. ANALYSIS

A comparison of the bearing-stress settlement curves for the strip footings with different widths and embedment depths is shown in Figure 10(a). The bearing stress-settlement curves for the two embedded baseline footings in Test QT-02 and QT-03 are very similar and are stiffer than the curve for the footing without embedment in Test QT-01. While the larger footing in Test QT-03 failed prematurely, it had a much stiffer bearing stress-settlement curve than the baseline footings. A comparison of the effect of footing shape is shown in Figure 10(b). The circular footings ended up having a greater bearing capacity than the strip footing, likely because strip footings have a greater zone of stress distribution than circular or square footings. A comparison of the effect of load inclination angle on the vertical components of the bearing stress-settlement curve is shown in Figure 10(a). The footings with a greater inclination of the footing load from the vertical had a reduction in stiffness and a lower ultimate bearing capacity.

A comparison of the failure response details of the footings in the eight tests is shown in Table 3. As the first two tests reached the maximum load of the actuator as tilting was limited, no ultimate bearing pressure is reported, while for the other tests the ultimate bearing stress is reported at the moment that tilting failure was observed. In addition, the bearing stresses at a serviceability limit state corresponding to a normalized settlement of 0.1B is also summarized in Table 3. While an engineering design of a footing in soil would typically consider both the bearing capacity and settlement response separately, the settlements of the footings in TDA at the ultimate bearing capacity are significant and should be avoided in engineering design. Using the bearing stress at a normalized settlement of 0.1B provides engineers an understanding of the capacity that can be used in sizing footings or thrust blocks for utilities. This method is also consistent with the simplified design procedure proposed by Mahgoub and El Naggar (2022) for Type A TDA which depends on a settlement limit. The choice of a normalized settlement of 0.1B is consistent with the settlements at bearing capacity failure of footings in soils. For example, Skempton (1951) observed that that required settlement ranges between 3 to 7% of the footing width for surface footings, and up to 15% for deep footings built on saturated clay. Vesic (1963) observed that that required settlement ranges between 5 to 15% of the footing width for surface footings, and up to 25% for deep footings built on sand. Accordingly, 10% of the footing width is deemed to be reasonable.

The bearing stiffness calculated using the bearing force at a normalized settlement of 0.1B is shown in Figure 11. The bearing stiffnesses in this figure confirm the general trends in the comparison of the bearing stress-settlement curves for the smaller strip footings in Figure 10, but care should be taken as the bearing stiffness in terms of force/settlement does not account for the role of footing size. Accordingly bearing "modulus" values calculated as the bearing stress at a normalized settlement of 0.1B are also included in this figure. Embedment leads to a significant increase in bearing stiffness of concrete footings, potentially due to the frictional restraint of the TDA on the sides of the footing. The width of strip footings also leads to a substantial increase in bearing stiffness, but only a slight increase in the bearing modulus. The circular footings have a lower bearing stiffness than strip footings due to their smaller area but have a much greater bearing modulus corresponding to their steeper bearing stress-settlement curve in Figure 10(b). The bearing stiffness and bearing modulus increase with the diameter of the circular footings. Increased loading inclination leads to a decrease in the bearing stiffness as well.

The ultimate bearing capacity values in Table 3 were compared with those predicted from the generalized bearing capacity equation of Hansen (1970) using the estimated average friction angles and unit weights for each layer of TDA summarized in Table 1. The generalized bearing capacity equation of Hansen (1970) for a drained frictional material like TDA is given as follows:

$$q_{ult,pred} = c'N_c s_c d_c i_c e_c + \sigma_{zD}' N_q s_q d_q i_q e_q + \frac{1}{2}\gamma' B N_\gamma s_\gamma d_\gamma i_\gamma e_\gamma \quad (1)$$

where c' is the drained cohesion of the TDA (equal to zero), σ_{zD}' is the surcharge stress above the base of the footing, γ' is the unit weight of the TDA, and B is the footing width. The bearing capacity factors can be determined as follows:

$$N_c = \frac{(N_q - 1)}{\tan\phi'}$$

$$N_q = e^{\pi \tan\phi'} \tan^2\left(45 + \frac{\phi'}{2}\right) \quad (2)$$

$$N_\gamma = 1.5(N_q - 1)\tan\phi'$$

where ϕ' is the secant friction angle of the TDA. Ghaaowd et al. (2018) found that the failure envelope for Type B TDA had a nonlinear shape, with a secant friction angle that decreases with increasing normal stress. Accordingly, to enable the use of the bearing capacity of Hansen (1970), the secant friction angle that was representative of the normal stress range in the experiments was used to estimate the bearing capacity. The secant friction angles in Table 1 were calculated for the mean effective stress at mid-depth in the TDA layer under the footing determined using the nonlinear failure envelope equation given in Ghaaowd et al. (2017). The shape factors are defined as follows:

$$s_c = 1 + (B/L)(N_q/N_c)$$

$$s_q = 1 + (B/L)\tan\phi' \quad (3)$$

$$s_\gamma = 1 - 0.4(B/L)$$

where B is the total width of the footing and L is the total length of the footing. While the footing in this study is meant to replicate a strip footing where L>B, the actual value of L is used in the analyses. The depth factors are defined as follows:

$$d_c = \left(d_q s_q N_q - 1\right)/\left[\left(N_q - 1\right)s_c\right]$$
$$d_q = 1 + 0.1(D/B) \tag{4}$$
$$d_\gamma = 1$$

where D is the embedment depth. The inclination factors are defined as follows:

$$i_c = (1 - \lambda/90)^2$$
$$i_q = (1 - \lambda/90)^2 \tag{5}$$
$$i_\gamma = (1 - \lambda/\phi')^2$$

where λ is the inclination of the applied load.

The predictions from the Hansen (1970) generalized bearing capacity equation for each of the tests are summarized in Table 3, and a comparison between the measured and predicted ultimate bearing capacity values is shown in Figure 12. Except for the large strip footing which may have failed prematurely, the ultimate bearing capacity values are reasonably well-predicted using the generalized bearing capacity equation using an average secant friction angle. The predicted bearing capacity values are very sensitive to the estimated friction angle and unit weight, which emphasizes the importance of having good estimates of these values when predicting bearing capacity in the field. A correlation between the predicted bearing capacity from Hansen (1970) and the bearing stress at a normalized settlement of 0.1B is also shown in Figure 12. This correlation is empirical, but it may be useful to practitioners hoping to estimate the bearing stress that can be relied upon prior to reaching failure due to serviceability concerns.

The constant load stages in Test QT-01 permit assessment of the short-term creep response of the TDA. While the duration of these constant load stages (5-15 minutes) is far shorter than usual in creep characterization tests, the creep settlements started to follow a stabilized trend with time as shown in Figure 13. The secondary compression or creep coefficients $C_{\alpha\varepsilon}$ shown in this figure were calculated using the average strain across the 3 m TDA layer and show some slight stress dependency with values ranging from 0.0049 to 0.0083. These values are slightly larger than the secondary creep coefficient of Type B TDA measured in a one-dimensional compression test by Yarahuaman and McCartney (2023) of 0.0029. While the time period permitted for creep in this study is very short compared to the duration of loading in the field, meaning that the creep coefficients should be used with caution, they may be useful for preliminary creep settlement estimates. Further, the creep coefficients from this study are in the middle of the range of creep coefficients for TDA from the literature by Wartman et al. (2007). The creep coefficients may be used in design following an approach similar to the method of Schmertmann (1970), where the creep settlement is calculated for a target time period. These creep settlements can be accounted for in the design of TDA fills using the overbuild approach of Humphrey (2008b).

Despite the large settlements observed in some of the experiments in this study, footings in TDA can still be designed with a given dimensions and embedment so that they can provide the necessary bearing capacity at a desired serviceability limit state. In most types of footings in the field, tilting is not restricted, so the bearing capacity equation of Hansen (1970) or the correlation for the serviceability limit state in Figure 12 can be used in design. For the case of rocking footings where the TDA is used as part of a geotechnical seismic isolation system, the bearing capacity at the serviceability limit state should be used in the calculations of the critical area during rocking to prevent overturning. For footings with restricted tilting, a hardening response with a punching shear failure mechanism is expected without a clear bearing capacity value within a reasonable settlement, so the stiffness of the bearing stress-settlement curves presented in this study can be used to estimate the bearing stress for a desired settlement at the serviceability limit state.

5. CONCLUSIONS

This study presented an evaluation of the bearing capacity of shallow footings in TDA to both provide a better insight into the roles of different variables like footing width, embedment depth, footing shape, and loading inclination, and to evaluate the role of predictions from bearing capacity equations using shear strength parameters from direct shear tests on TDA. The trends in the bearing stress-settlement curves with the footing width, embedment depth, footing shape, and loading inclination were consistent with expectations from past studies on footings in soils. Further, the ultimate bearing capacity was well predicted using a generalized bearing capacity equation with the average secant friction angle for the TDA layer beneath the footing. However, the footing settlements at bearing capacity were much larger than expected for footings in soils. A correlation was developed to provide practitioners guidance on the expected bearing stresses that could be mobilized at a serviceability limit state corresponding to normalized settlements of 10% of the footing width. The TDA layer was also observed to deform slightly differently from granular soils around footings, with a drag-down effect in the TDA near the footing edges. The TDA was also observed to absorb large surficial settlements across its depth, confirming its suitability for use as a bridging material for pipelines or utilities. While creep settlements were observed during footing loading, the magnitudes of the creep coefficient were consistent with measurements from element-scale tests on TDA.

ACKNOWLEDGEMENTS

The authors appreciate support from CalRecycle under contract DRR20081. The authors thank Joaquin Wright from GHD and Stacey Patenaude and Mustafe Botan from CalRecyle for their support. The authors also thank the staff of the UCSD Powell Laboratories including Michael

Sanders, Noah Aldrich, Michael Dyson, Pablo Garcia, Zackary Kamibayashiyama, and Alejandro Ibarra for their input and support during construction and testing.

DATA AVAILABILITY STATEMENT

All data, models, and code generated or used during the study appear in the article.

NOTATIONS

B	footing width (m)
c'	drained cohesion of TDA (Pa)
$C_{\alpha\varepsilon}$	creep coefficient (dimensionless)
D	footing embedment depth
L	footing length (m)
d_c	depth factor (dimensionless)
d_q	depth factor (dimensionless)
d_γ	depth factor (dimensionless)
e_c	eccentricity factor (dimensionless)
e_q	eccentricity factor (dimensionless)
e_γ	eccentricity factor (dimensionless)
i_c	inclination factor (dimensionless)
i_q	inclination factor (dimensionless)
i_g	inclination factor (dimensionless)
N_c	bearing capacity factor (dimensionless)
N_q	bearing capacity factor (dimensionless)
N_g	bearing capacity factor (dimensionless
q_{ult}	measured ultimate bearing capacity (Pa)
$q_{S=0.1B}$	bearing stress at a settlement of 0.1B (Pa)
$q_{ult,pred}$	predicted ultimate bearing capacity (Pa)
S	footing settlement (m)
s_c	shape bearing factor (dimensionless)
s_q	shape bearing factor (dimensionless)
s_γ	shape bearing factor (dimensionless)
z	depth from surface (m)
ϕ'	friction angle (°)
γ'	unit weight of TDA (N/m^3)
λ	inclination of applied load (°)
σ_{zd}'	overburden stress (Pa)

ABBREVIATIONS

TDA Tire Derived Aggregate

REFERENCES

Adesokan, D., Fleming, I., and Hammerlindl, A. (2020). "One-dimensional (1D) immediate compression and creep in large particle-sized tire-derived aggregate (TDA) for leachate collection and removal systems (LCRSs)." Can. Geotech. J. 58: 982-994.

Ahn, I.-S., and Cheng, L. (2014). "Tire derived aggregate for retaining wall backfill under earthquake loading." Construction and Building Materials. 57: 105-116.

Arefnia, A., Dehghanbanadaki, A., and Kassim, K. A. (2021). "Ultimate bearing capacity of strip footing resting on clay soils mixed with tire-derived aggregates". Front. Struct. Civ. Eng. 15(4): 1016-1024.

ASTM. (2020). "Standard practice for use of scrap tires in civil engineering applications." ASTM D6270, West Conshohocken, PA.

CalRecycle (California Department of Resources Recycling and Recovery). (2022). "California waste tire market report: 2021." DRRR-2022-1712, Sacramento, CA.

Chenari, J. R., Fatahi, B., Akhavan Maroufi, M. A., and Alaie, R. (2017). "An experimental and numerical investigation into the compressibility and settlement of sand mixed with TDA". Geotech. Geol. Eng. 35: 2401-2420.

Gajan, S. and Kutter, B.L. (2008). "Effect of critical contact area ratio on moment capacity of rocking shallow footings." Geotechnical Earthquake Engineering and Soil Dynamics IV, Sacramento, CA. 18-22 May. DOI: 10.1061/40975(318)133.

Deng, L, and Kutter, B.L. (2012). "Characterization of rocking shallow foundations using centrifuge model tests." Earthquake Engineering & Structural Dynamics, 41(5), 1043-1060.

Drescher, A., and Newcomb, D.E. (1994). "Development of design guidelines for use of shredded tires as a lightweight fill in road subgrade and retaining walls." Report No. MN/RC-94/04, Dept. of Civil and Mineral Engineering, Univ. of Minnesota, Minneapolis.

El Naggar, H., Soleimani, P., and Fakhroo. A. (2016). "Strength and stiffness properties of green lightweight fill mixtures." Geotechnical and Geological Engineering 34: 867–876.

Fox, P. J., Sander, A. C., Elgamal, A., Greco, P., Isaacs, D., Stone, M., & Wong, S. (2015). Large soil confinement box for seismic performance testing of geo-structures. Geotechnical Testing Journal, 38(1), 72-84.

Fox, P.J., Thielmann, S.S., Sanders, M.J., Latham, C., Ghaaowd, I., and McCartney, J. S. (2018). "Large-scale combination direct shear/simple shear device for tire-derived aggregate." ASTM Geotechnical Testing Journal. 41(2): 340-353.

Ghaaowd, I. and McCartney, J.S. (2020). "Pullout of geogrids from tire derived aggregate with large particle size." Geosynthetics International. 27(6), 671-684.

Ghaaowd, I., Fox, P.J. and McCartney, J.S. (2020). "Shearing behavior of the interfaces between tire derived aggregate and three soil materials." ASCE Journal of Materials in Civil Engineering. 32(6): 04020120.

Ghaaowd, I., McCartney, J.S., Thielmann, S., Sanders, M. and Fox, P.J. (2017). "Shearing behavior of tire derived aggregate with large particle sizes. I: Internal and concrete interface direct shear behavior." ASCE Journal of Geotechnical and Geoenvironmental Engineering. 143(10): 04017078.

Hansen, J.B. (1970). "A revised and extended formula for bearing capacity". Danish Geotechnical Institute, 28: 5-11.

Hoppe, E.J. (1994). “Field study of shredded-tire embankment.” Report No. FHWA/VA-94-IR1, Virginia Dept. of Transportation, Richmond, VA.

Humphrey, D.N. (2008a). Civil Engineering Application of Tire Derived Aggregate. Alberta Recycling Management Authority, Edmonton, AB, Canada.

Humphrey, D.N. (2008b). “Tire derived aggregate as lightweight fill for embankments and retaining walls.” Scrap Tire Derived Geomaterials – Opportunities and Challenges. Hazarika and Yasuhara (eds). Taylor and Francis, London. 59-81.

Mahgoub, A., and El Naggar, H., (2020). “Shallow foundation on lightweight TDA backfill: Field tests and 3D numerical modelling.” Computers and Geotechnics. 126: 103761

Mahgoub, A., and El Naggar, H., (2022). “Using TDA underneath shallow foundations: simplified design procedure.” International Journal of Geotechnical Engineering, 16(7): 787-801.

McCartney, J.S. (2021). Design of Mechanically Stabilized Tire Derived Aggregate (MSTDA) Retaining Walls. Report DRRR-2023-1717 to CalRecycle. 97 p.

McCartney, J.S., Ghaaowd, I., Fox, P.J., Sanders, M., Thielmann, S., and Sander, A. (2017). “Shearing behavior of tire derived aggregate with large particle sizes. II: Cyclic simple shear behavior.” Journal of Geotechnical and Geoenvironmental Engineering. 143(10): 04017079.

Meles, D., Bayat, A., and Chan, D. (2014). “One-dimensional compression model for tire-derived aggregate using large-scale testing apparatus.” International Journal of Geotechnical Engineering, 8(2): 197-204.

Mills, B., and McGinn, J. (2010). “Design, construction, and performance of highway embankment failure repair with tire-derived aggregate.” Transportation Research Record 1345: 90–99.

Schmertmann, J.H. (1970). "Static cone to compute static settlement over sand." J. Soil Mech. & Found. Div., ASCE, 96(SM3): 7302-1043.

Senetakis, K., Anastasiadis, A., Pitilakis, K. (2012). "Dynamic properties of dry sand/rubber (SRM) and gravel/rubber (GRM) mixtures in a wide range of shearing strain amplitudes." Soil Dynamics and Earthquake Engineering 33(1): 38-53.

Skempton, A.W. (1951). "The bearing capacity of clays." Proc. Bldg. Res. Conf., 1951. 1: 180.

Tandon, V., Velazco, D.A., Nazarian, S., and Picornell, M. (2007). "Performance monitoring of embankment containing tire chips: Case study." J. Perform. Const. Fac., 21(3): 207–214.

Tsang, H., Lo, S. H., Xu, X., and Neaz Sheikh, M. (2012). "Seismic isolation for low-to-medium-rise buildings using granulated rubber-soil mixtures: numerical study." Earthquake Eng. Struct. Dyn. 41: 2009-2024.

Tsang, H., Tran, D., Hung, W., Pitilakis, K., and Gad, E.F. (2020). "Performance of geotechnical seismic isolation system using rubber-soil mixtures in centrifuge testing". Earthquake Engineering & Structural Dynamics. 50: 1271-1289.

Tweedie, J.J., Humphrey, D.N., and Sandford, T.C. (1998). "Full scale field trials of tire shreds as lightweight retaining wall backfill, at-rest condition." Proc. Transportation Research Board 1998 Annual Meeting, Washington, DC.

Vesic, A. (1963). "Bearing capacity of deep foundations in sand". Highway Res. B., 39: 112-153.

Vesic, A. (1973). "Analysis of ultimate loads on shallow foundations". Journal of the Soil Mechanics and Foundation Division, 99(1): 45-73.

Wartman, J., Natale, M. F., and Strenk, P. M. (2007). "Immediate and time-dependent compression of tire derived aggregate." Journal of Geotechnical and Geoenvironmental Engineering 133(3): 245–56.

Yarahuaman, A. and McCartney, J.S. (2023). “Large-scale testing of the static one-dimensional compression response of tire-derived aggregate.” GeoCongress 2023. Los Angeles, CA. Mar. 26-29. GSP 341. ASCE, Reston, VA. 593-603.

Yarahuaman, A., and McCartney, J.S. (2024). “Large-scale seismic response testing of shallow foundations embedded in tire-derived aggregate for geotechnical seismic isolation.” Soil Dynamics and Earthquake Engineering. 177: 108417. DOI: 10.1016/j.soildyn.2023.108417.

Table 1. Summary of quasi-static testing specimen details

Specimen	Thickness of TDA layer [m]	Footing width or diameter, *B* [m]	Footing length, *L* [m]	Footing embedment, *D* [m]	Average TDA layer unit weight, γ' [kN/m^3]	Estimated TDA layer ϕ' [°]
QT-01	3.00	0.46	2.13	0.00	6.25	38.0
QT-02	3.00	0.46	2.13	0.46	6.77	39.0
QT-03	3.00	0.46	2.13	0.46	7.40	35.0
QT-04	3.00	0.91	2.13	0.91	7.10	35.0
QT-05	3.00	0.46	---	0.30	7.85	33.0
QT-06	3.00	0.30	---	0.30	8.02	31.0
QT-07	3.00	0.46	2.13	0.46	8.10	30.0
QT-08	3.00	0.46	2.13	0.46	8.18	30.0

Table 2. Summary of experimental protocol

Specimen	Testing control type	Load inclination from vertical, λ [°]	Number of actuators	Tilting restraint	Loading or displacement rate	Unloading or displacement rate
QT-01	Load-control	0	1	Partial	8.89 kN/min	8.89 kN/min
QT-02	Displacement-control	0	2	Restrained	12.7 mm/min	12.7 mm/min
QT-03	Load-control	0	2	None	8.89 kN/min	17.79 kN/min
QT-04	Load-control	0	2	None	8.89 kN/min	17.79 kN/min
QT-05	Displacement-control	0	1	None	12.7 mm/min	12.7 mm/min
QT-06	Displacement-control	0	1	None	12.7 mm/min	12.7 mm/min
QT-07	Displacement-control	30	1	None	12.7 mm/min	12.7 mm/min
QT-08	Displacement-control	60	1	None	12.7 mm/min	12.7 mm/min

Table 3. Summary of quasi-static test results on footings in Type B TDA (N/A = Not applicable)

Specimen	Reason to stop loading	Failure mode	Bulging of adjacent TDA	Ultimate bearing pressure, q_{ult} [kPa]	Bearing pressure at settlement criterion, $q_{S=0.1B}$ [kPa]	Predicted ultimate bearing pressure, $q_{u,pred}$ [kPa]
QT-01	Max. load of actuator	Punching shear	No	N/A	28	74
QT-02	Max. load of actuators	Punching shear	No	N/A	44	320
QT-03	Excess tilting	Punching shear	No	238	42	195
QT-04	Excess tilting	Punching shear	No	153	90	398
QT-05	Excess tilting	Punching shear	No	130	75	133
QT-06	Excess tilting	Punching shear	No	64	48	100
QT-07	Excess tilting	Punching shear	No	48	24	38
QT-08	Excess tilting	Punching shear	Yes	27	18	35

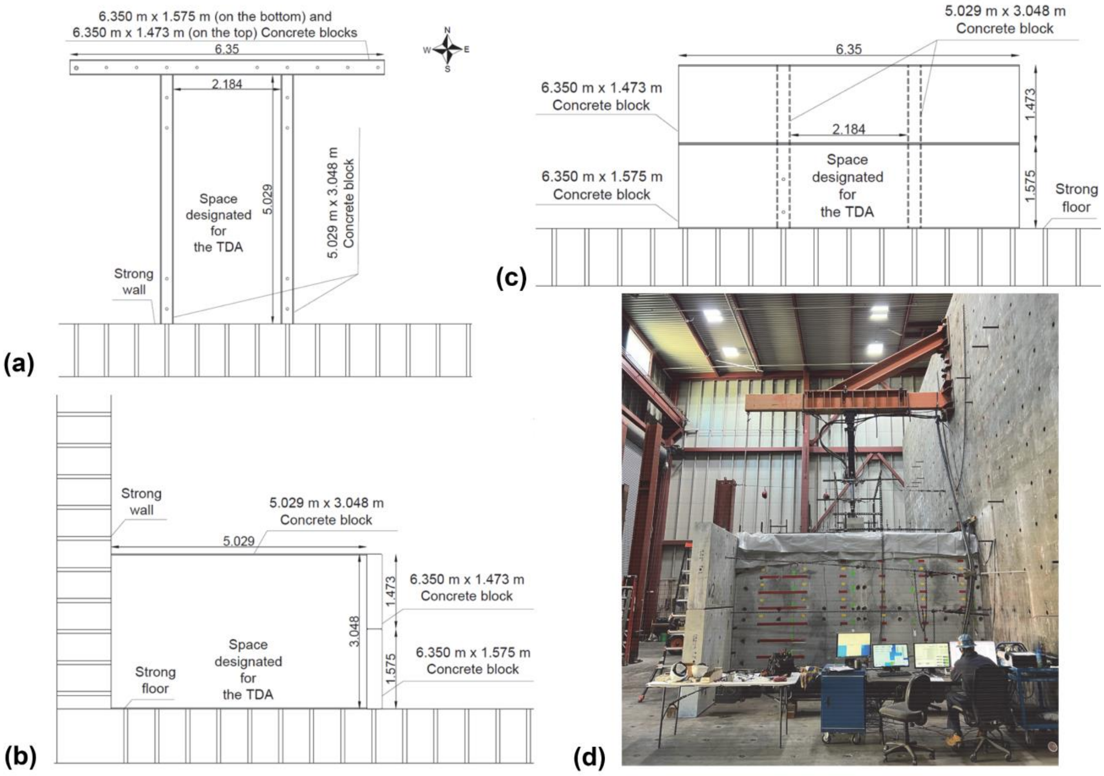

FIG. 1. Container used for foundation loading in TDA: (units in m): (a) Plan view, (b) Front view, (c) Side view, (d) Picture of container and loading frame attached to strong wall.

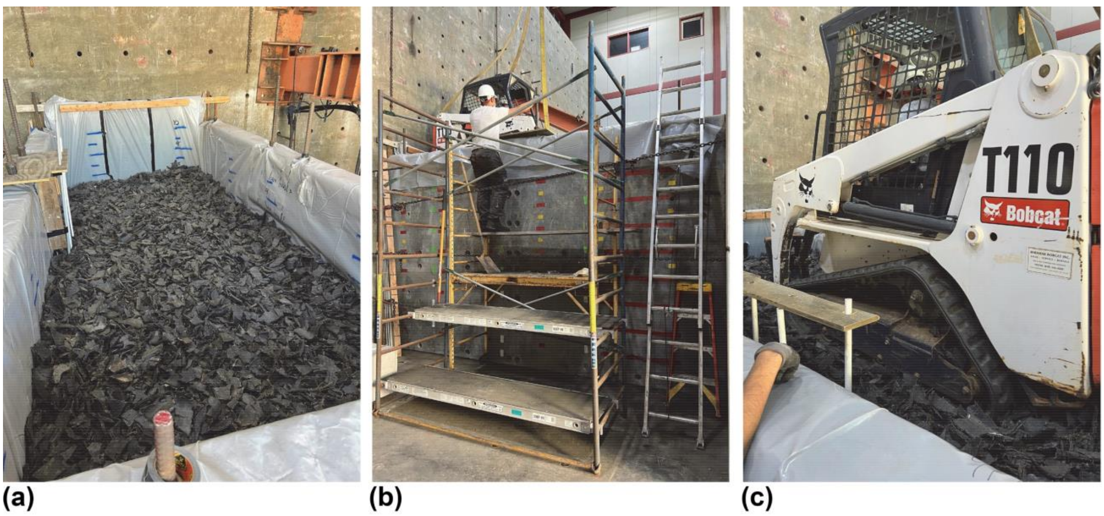

FIG. 2. TDA compaction procedures: (a) Leveling of TDA lift showing visquine sheeting on boundaries and embedded instrumentation; (b) Lowering skid steer onto TDA layer for compaction; (c) Compaction with skid steer.

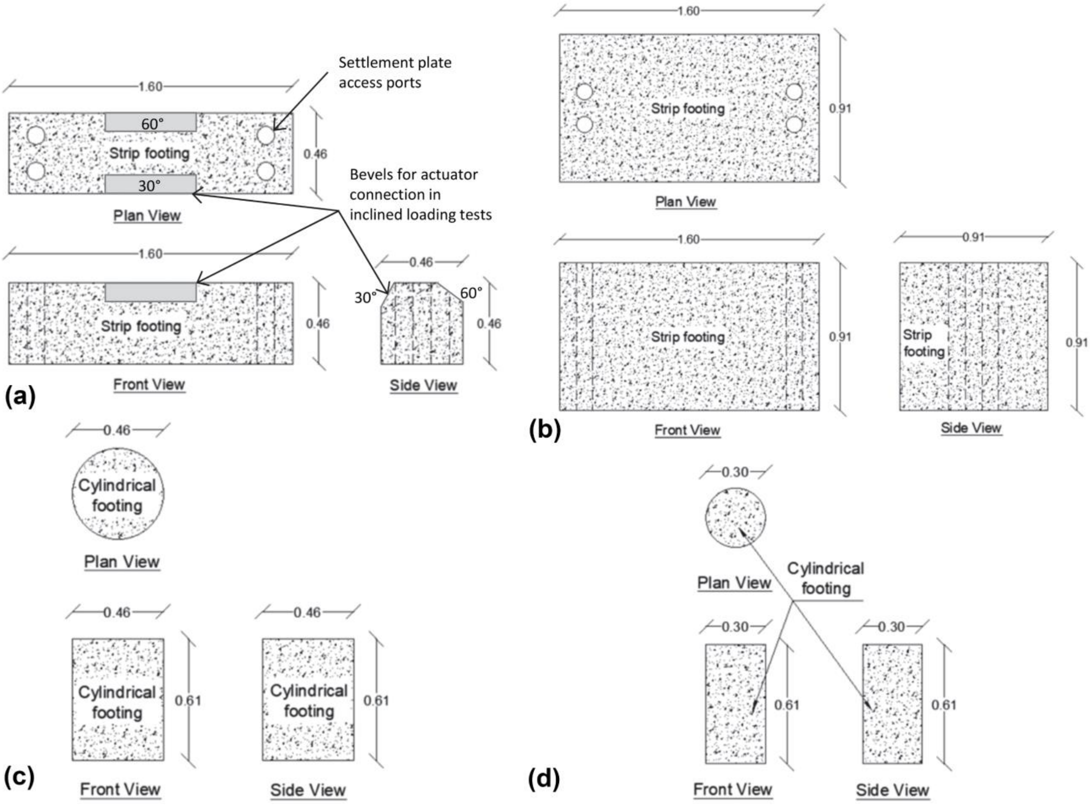

FIG. 3. Dimensions of shallow foundations: (a) Strip footing No 01; (b) Strip footing No 02; (c) Cylindrical footing No 01; (d) Cylindrical footing No 02.

FIG. 4. Pictures of selected tests: (a) Test QT-01 on vertically-loaded surficial small strip footing; (b) Test QT-03 on vertically loaded embedded small strip footing; (c) Test QT-04 on vertically-loaded embedded large strip footing; (d) Test QT-05 on vertically-loaded embedded cylindrical footing; (e) Test QT-07 on inclined-loaded embedded strip footing; (f) Test QT-08 on inclined-loaded embedded strip footing.

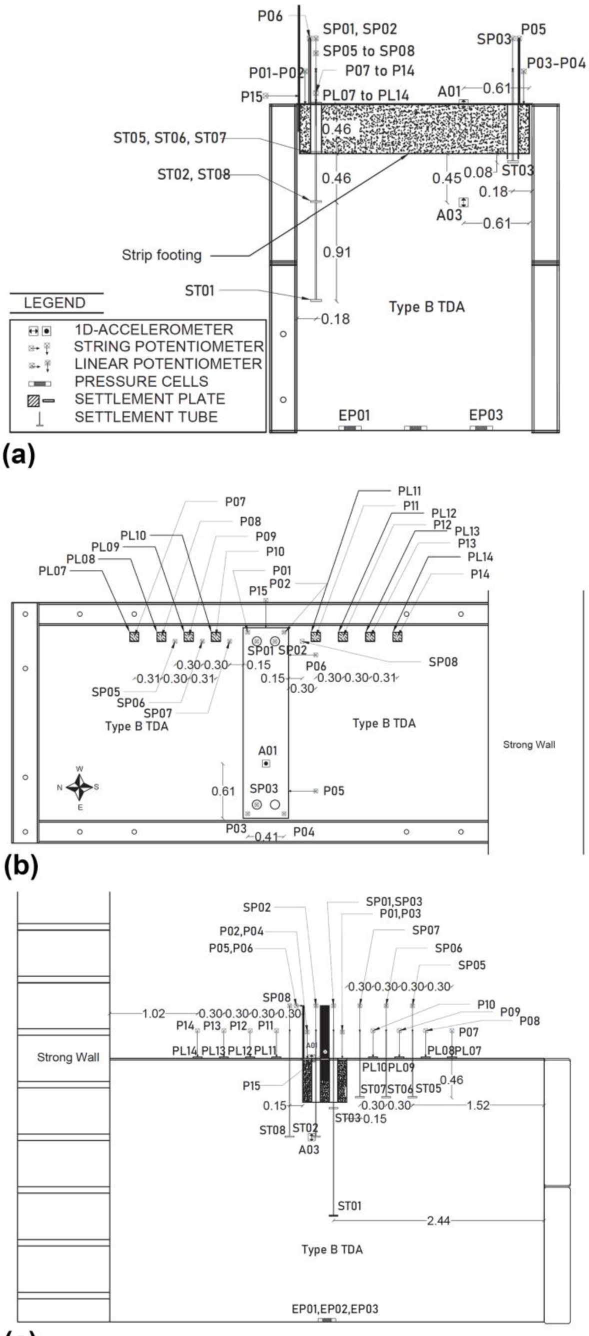

FIG. 5. Typical instrumentation layouts for Test QT-03: (a) Front section; (b) Plan; (c) Side section

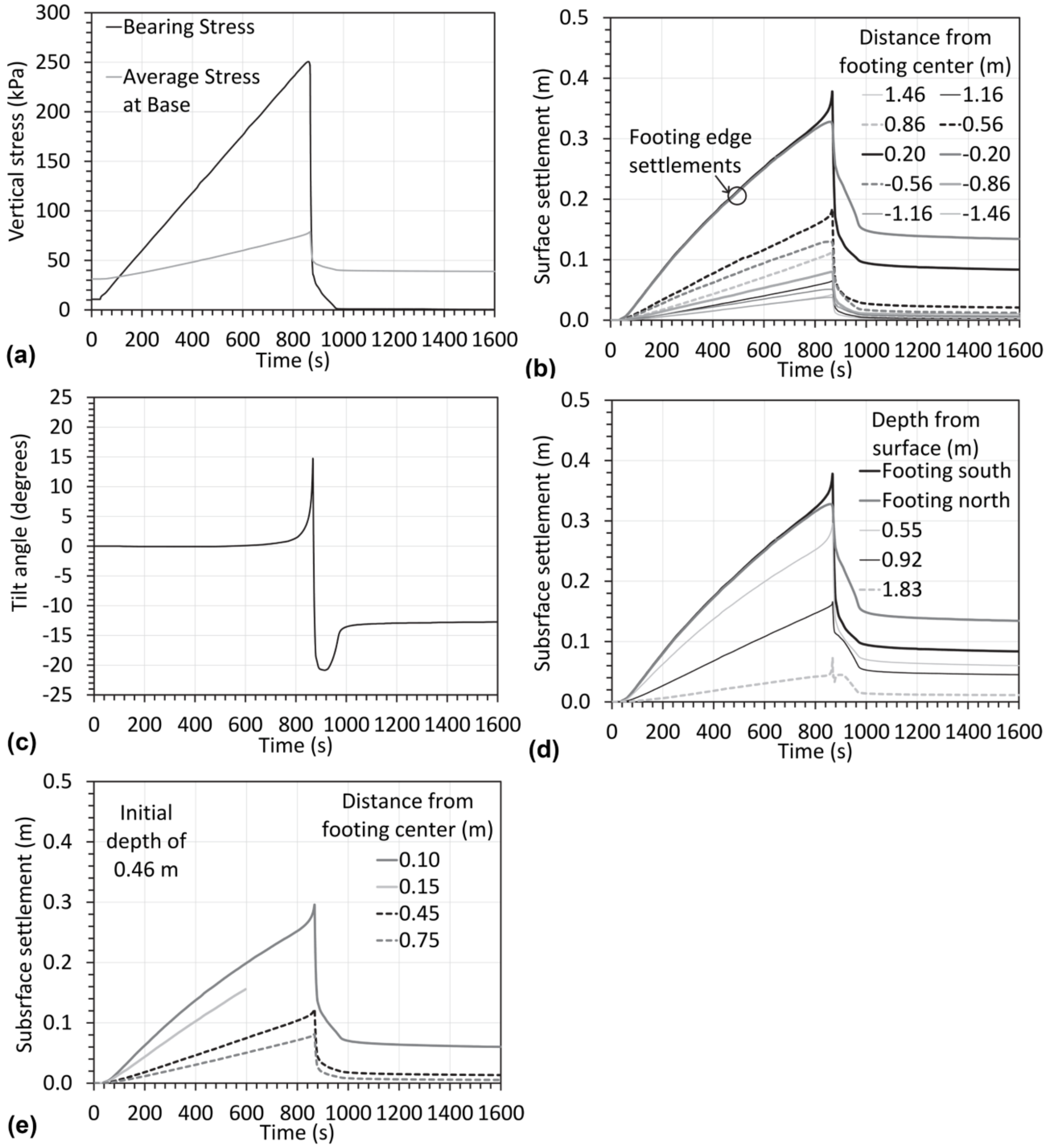

FIG. 6. Time series for a typical test (Test QT-03, B=0.48 m): (a) Applied bearing stress and average vertical stress at the base of the container; (b) Surface TDA settlements; (c) Tilting; (d) Subsurface TDA settlements below footing; (e) Subsurface TDA settlements outside footing.

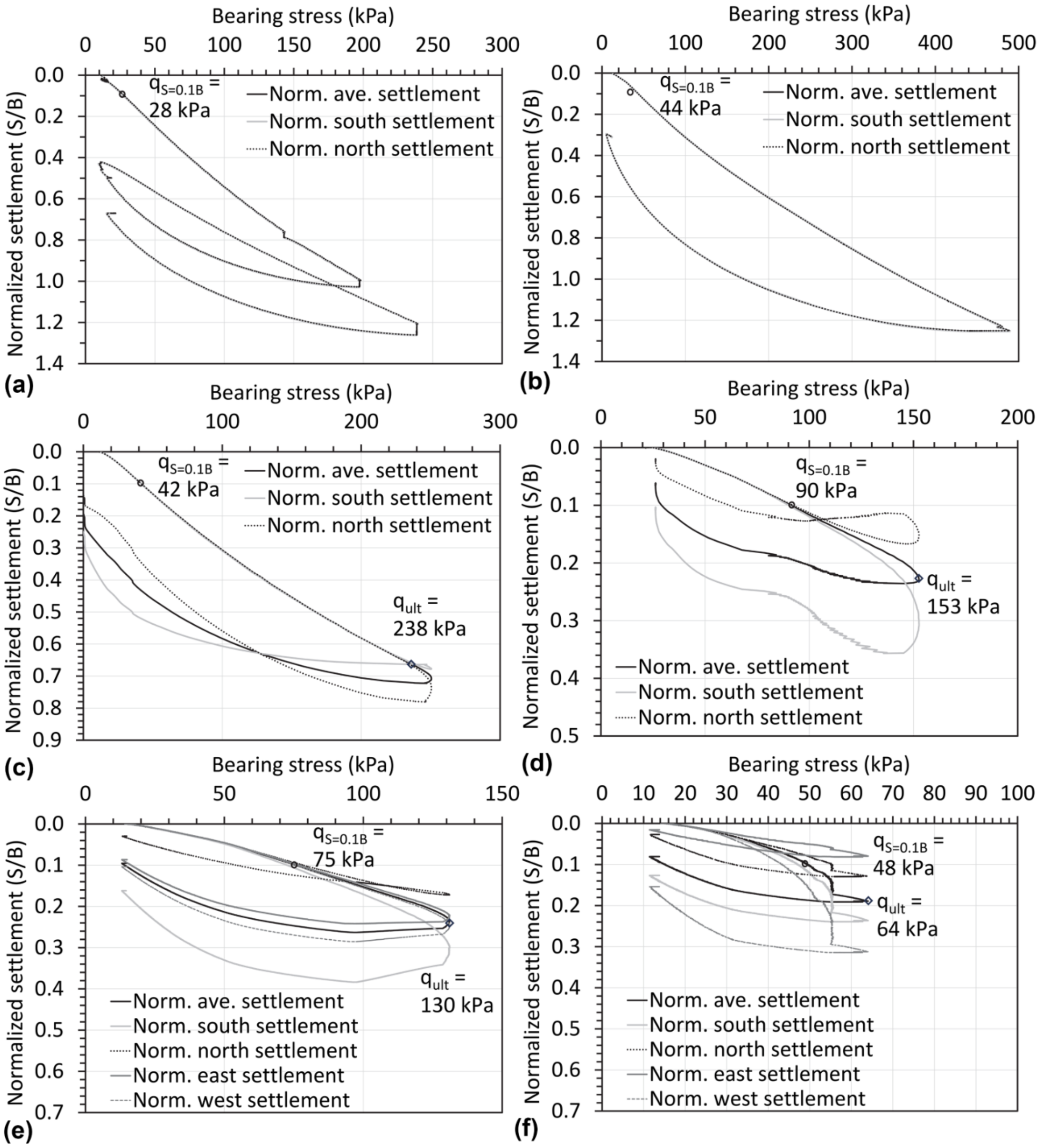

FIG. 7. Settlement-stress response for vertically-loaded footings: (a) Test QT-01; (b) Test QT-02; (c) Test QT-03; (d) Test QT-04; (e) Test QT-05; (f) Test QT-06.

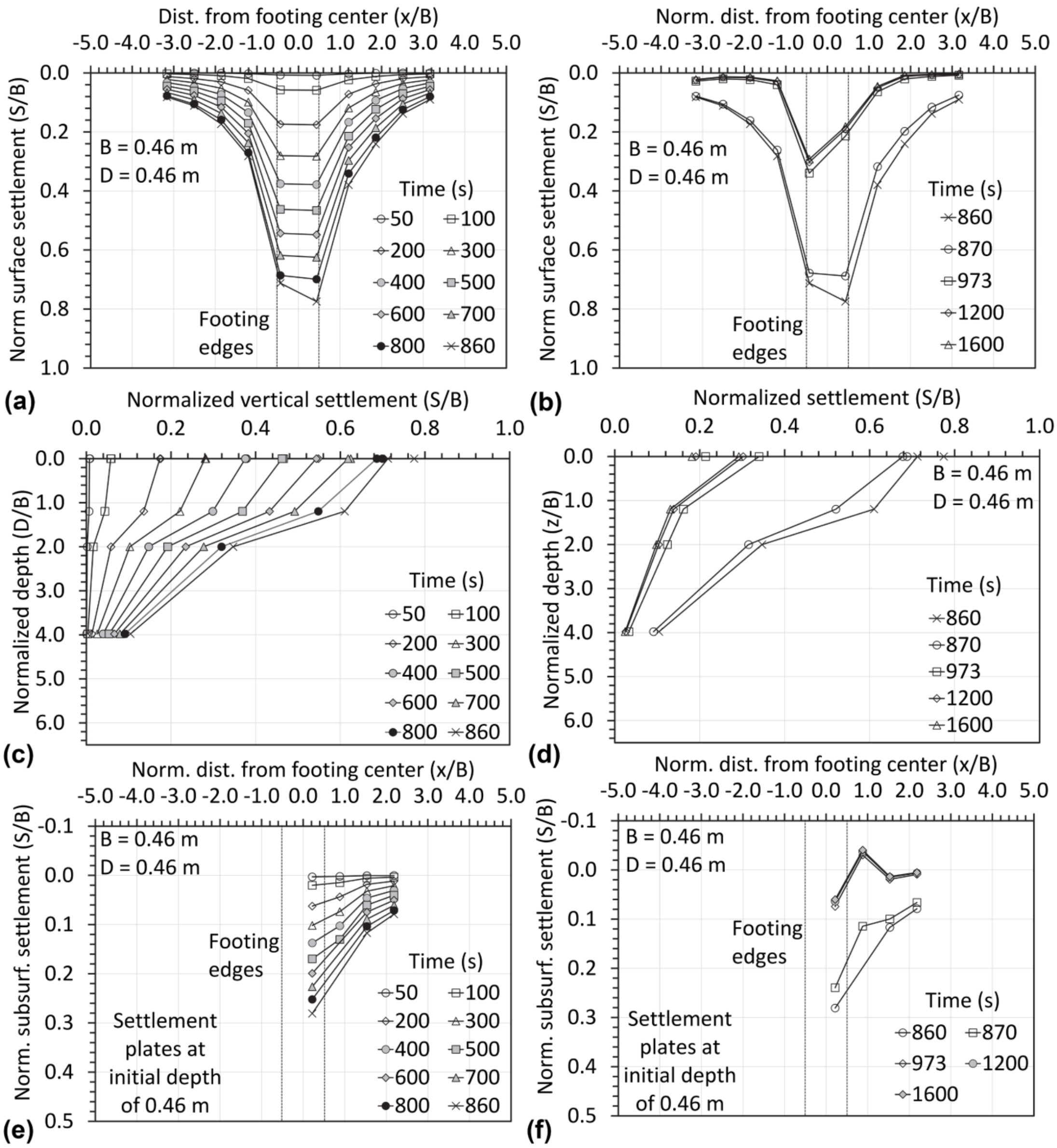

FIG. 8. Examples of profile plots of TDA deformation during foundation loading in Test QT-03: (a) Surface settlements during loading; (b) Surface settlements during unloading; (c) Subsurface settlements during loading; (d) Subsurface settlements during unloading; (e) Subsurface settlements during loading; (b) Subsurface settlements during unloading.

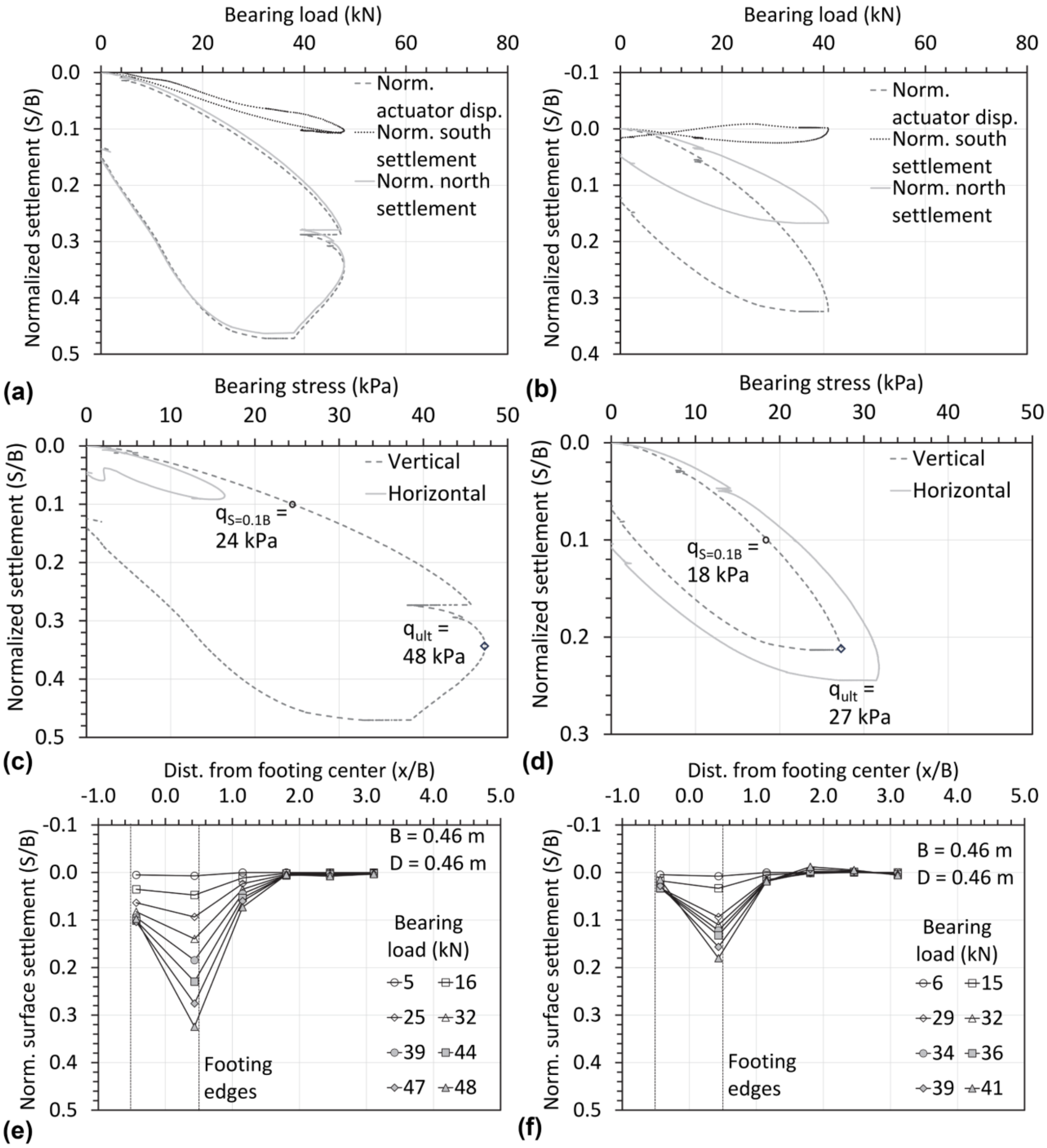

FIG. 9. Analysis of inclined footing tests: (a) Force-displacement for Test QT-07; (b) Force-displacement for Test QT-08; (c) Vertical and horizontal stress-displacement for Test QT-07; (d) Vertical and horizontal stress-displacement for Test QT-08; (e) TDA surface deformations in Test QT-07; (f) TDA surface deformations in Test QT-07.

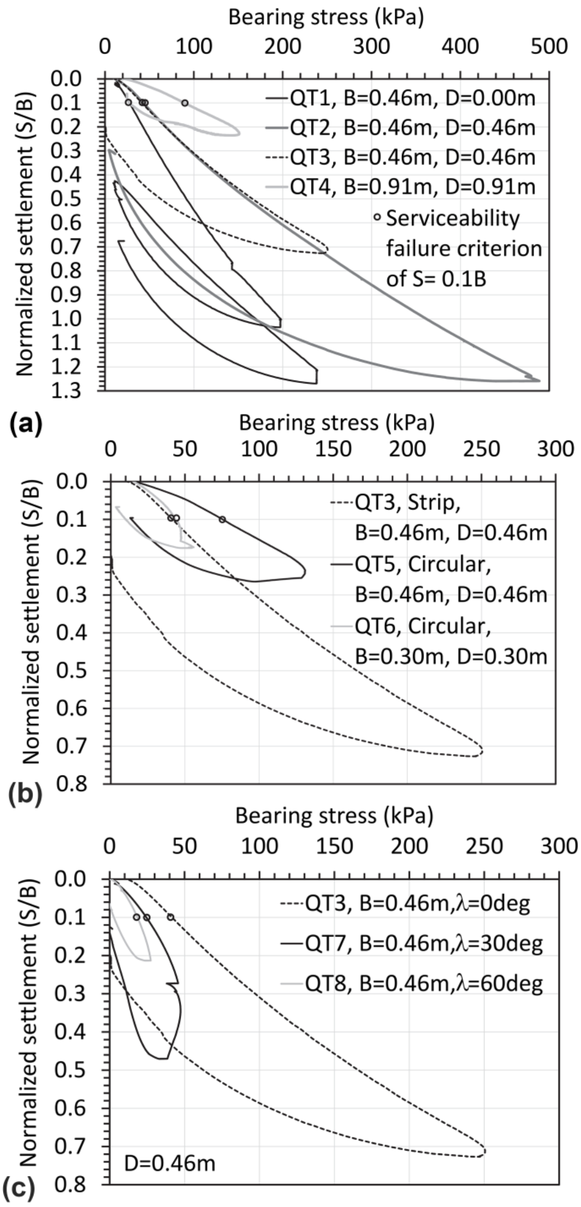

FIG. 10. Comparisons of stress-settlement curves for different tests; (a) Effects of strip footing dimensions and embedment; (b) Effects of footing shape; (c) Effects of load inclination.

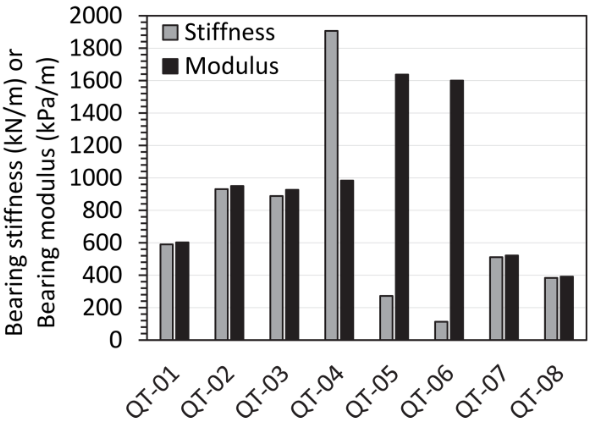

FIG. 11. Bearing stiffness and bearing "modulus" for the different footings.

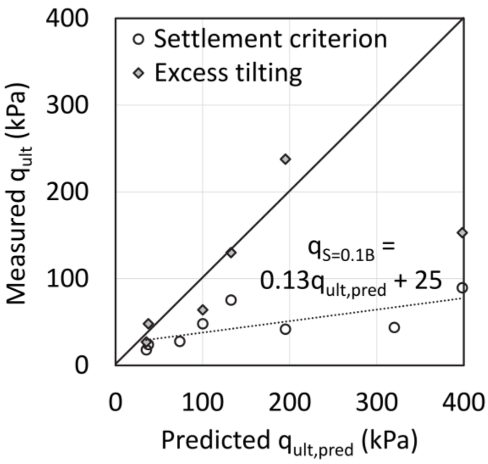

FIG. 12. Measured vs. predicted ultimate bearing capacity for the different footings.

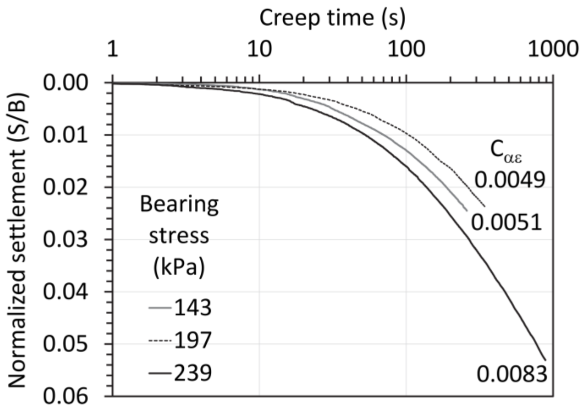

FIG. 13. Assessment of creep settlements under different bearing stresses applied to the strip footing in Test QT-01 along with average secondary creep coefficients.

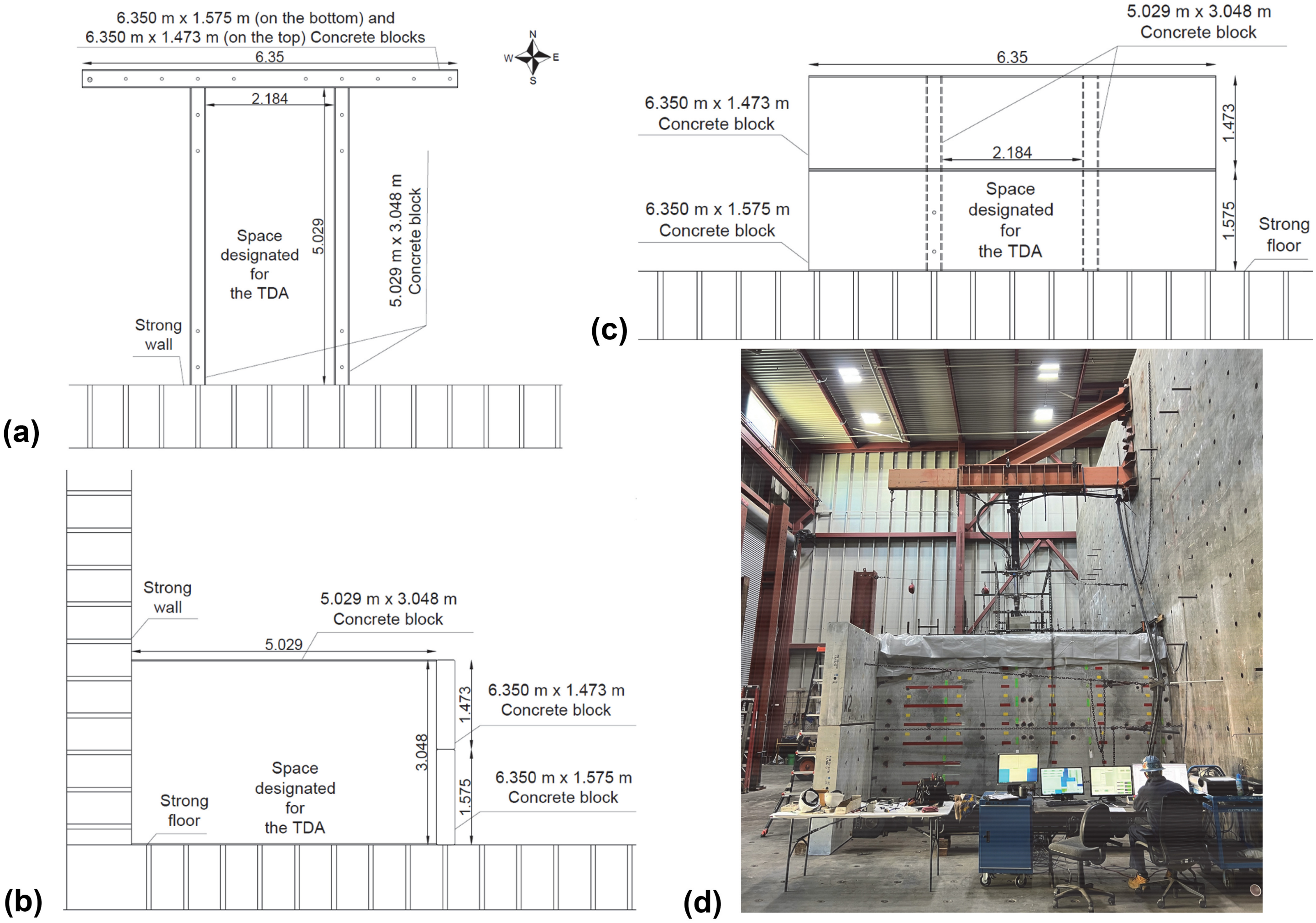
6.350 m x 1.575 m (on the bottom) and
6.350 m x 1.473 m (on the top) Concrete blocks
6.35
2.184
N
W
E
S
Space
designated
for
the TDA
5.029
5.029 m x 3.048 m
Concrete block
Strong
wall
(a)
Strong
wall
5.029 m x 3.048 m
Concrete block
5.029
1.473
3.048
6.350 m x 1.473 m
Concrete block
6.350 m x 1.575 m
Concrete block
1.575
Strong
floor
Space
designated
for
the TDA
(b)
5.029 m x 3.048 m
Concrete block
6.35
6.350 m x 1.473 m
Concrete block
2.184
1.473
6.350 m x 1.575 m
Concrete block
Space
designated
for
the TDA
1.575
Strong
floor
(c)
(d)

(a) (b) (c)

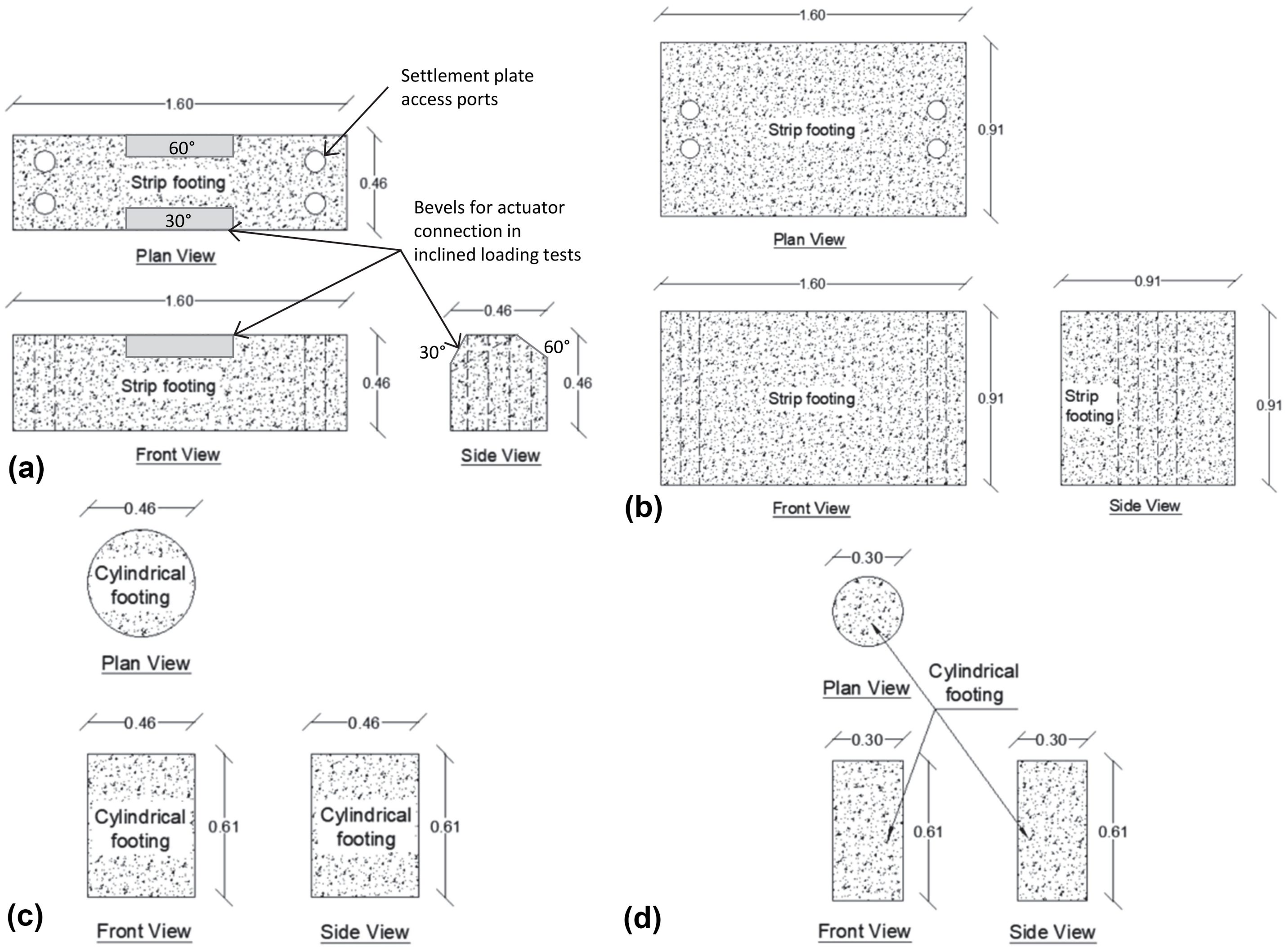
Settlement plate
access ports
1.60
60°
Strip footing
30°
0.46
Bevels for actuator
connection in
inclined loading tests
Plan View
1.60
0.46
30°
60°
Strip footing
0.46
0.46
Front View
Side View
(a)
1.60
Strip footing
0.91
Plan View
1.60
0.91
Strip footing
0.91
Strip
footing
0.91
(b)
Front View
Side View
0.46
Cylindrical
footing
Plan View
0.46
0.46
Cylindrical
footing
0.61
Cylindrical
footing
0.61
(c)
Front View
Side View
0.30
Plan View
Cylindrical
footing
0.30
0.30
0.61
0.61
(d)
Front View
Side View


(a)
(b)
(c)
(d)
(e)
(f)

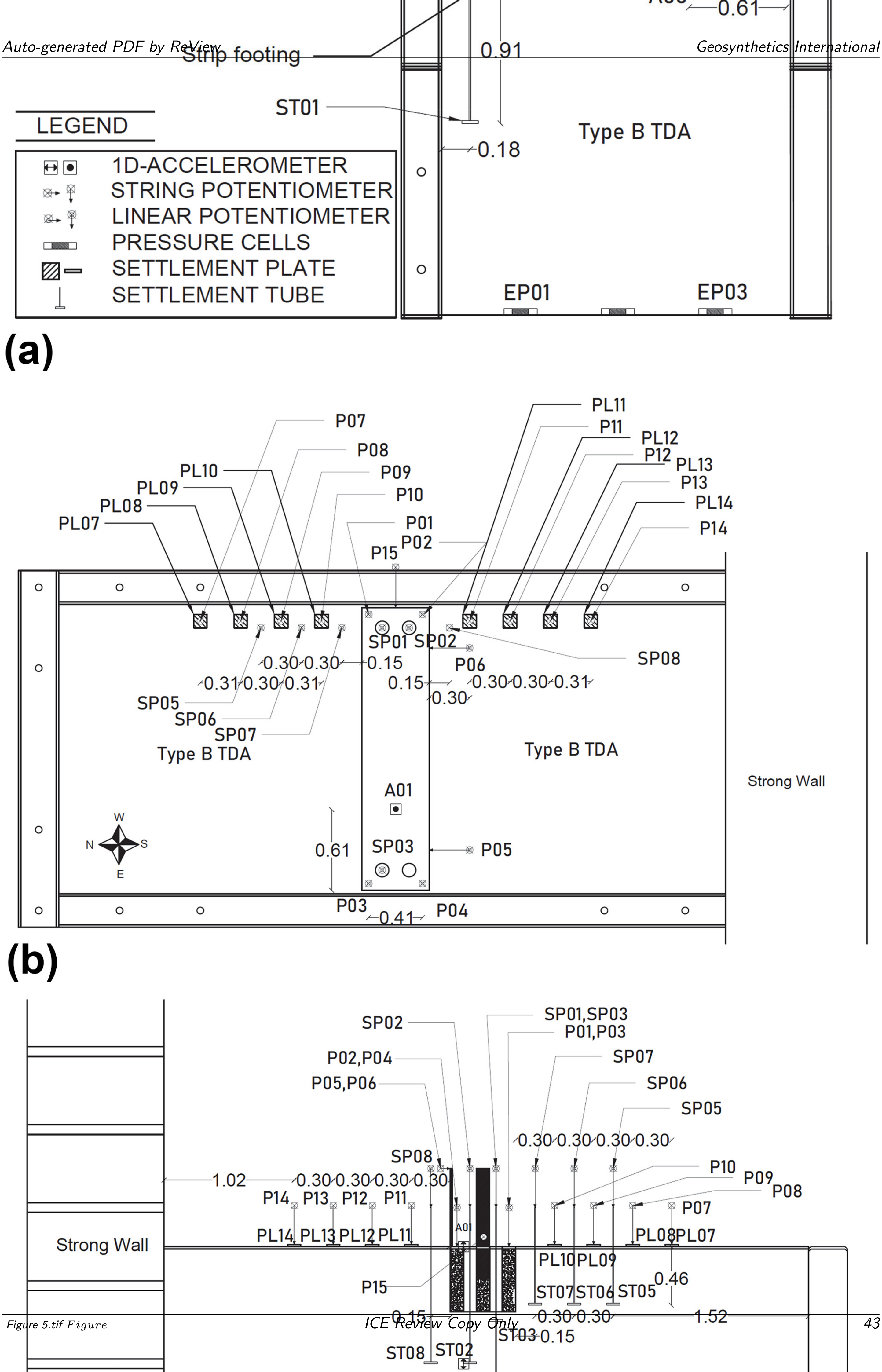

Strip footing
ST01
0.91
0.61
0.18
Type B TDA
LEGEND
1D-ACCELEROMETER
STRING POTENTIOMETER
LINEAR POTENTIOMETER
PRESSURE CELLS
SETTLEMENT PLATE
SETTLEMENT TUBE
EP01
EP03
(a)
PL11
P11
PL12
P12
PL13
P13
PL14
P14
P07
P08
P09
P10
PL10
PL09
PL08
PL07
P01
P02
P15
SP01 SP02
SP08
P06
0.30 0.30 0.15
0.31 0.30 0.31
0.15
0.30 0.30 0.31
0.30
SP05
SP06
SP07
Type B TDA
Type B TDA
Strong Wall
A01
W
N
S
E
0.61
SP03
P05
P03
P04
0.41
(b)
SP02
SP01,SP03
P01,P03
P02,P04
SP07
P05,P06
SP06
SP05
0.30 0.30 0.30 0.30
SP08
1.02
0.30 0.30 0.30 0.30
P10
P09
P08
P14 P13 P12 P11
P07
PL14 PL13 PL12 PL11
A01
PL08 PL07
Strong Wall
PL10 PL09
P15
0.46
ST07 ST06 ST05
0.15
0.30 0.30
1.52
ST03 0.15
ST08 ST02

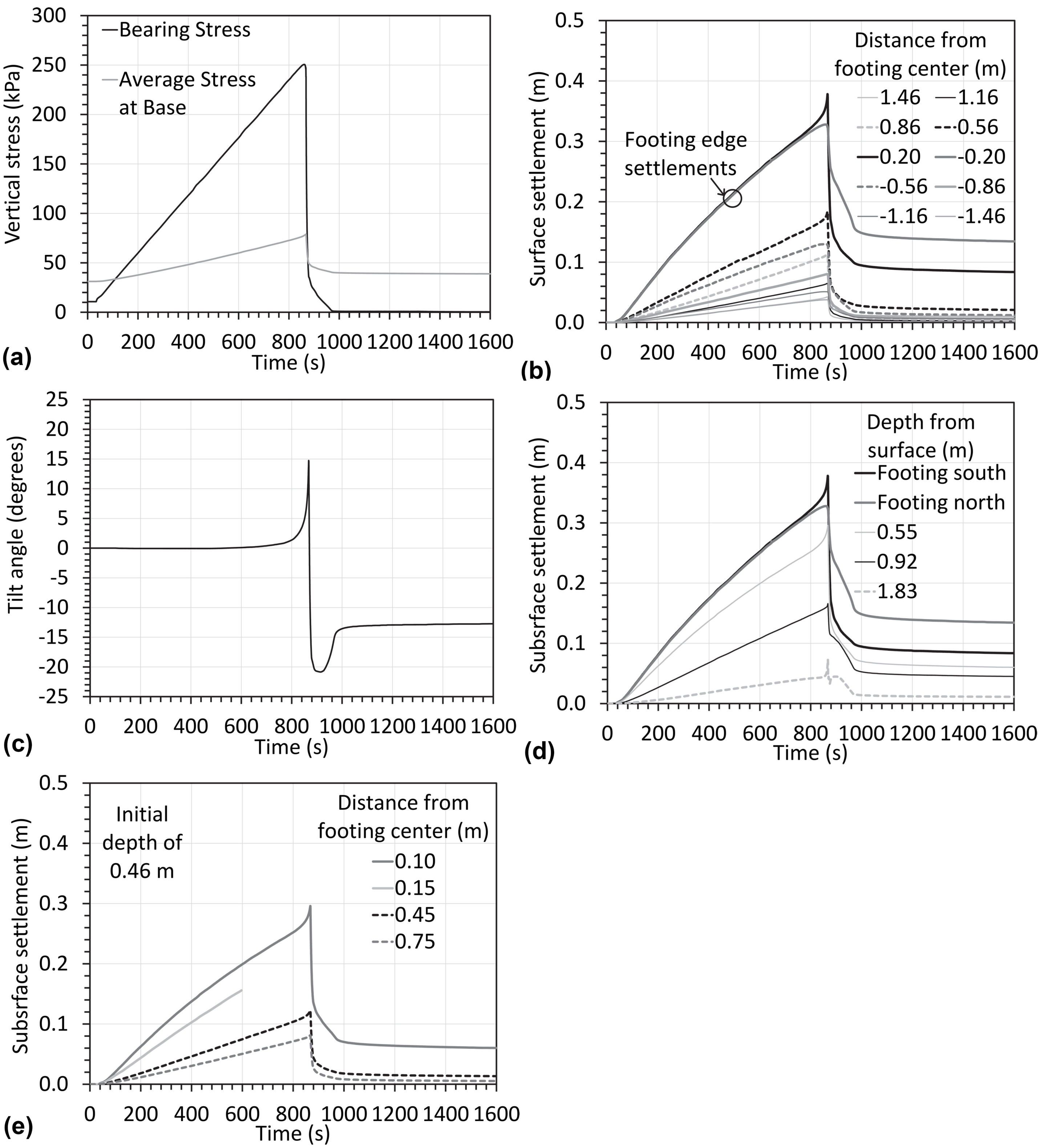

(a)
Vertical stress (kPa)
300
250
200
150
100
50
0
—Bearing Stress
—Average Stress at Base
0 200 400 600 800 1000 1200 1400 1600
Time (s)
(b)
Surface settlement (m)
0.5 0.4 0.3 0.2 0.1 0.0
Distance from footing center (m)
1.46 1.16
0.86 0.56
0.20 -0.20
-0.56 -0.86
-1.16 -1.46
Footing edge settlements
0 200 400 600 800 1000 1200 1400 1600
Time (s)
(c)
Tilt angle (degrees)
25 20 15 10 5 0 -5 -10 -15 -20 -25
0 200 400 600 800 1000 1200 1400 1600
Time (s)
(d)
Subsrface settlement (m)
0.5 0.4 0.3 0.2 0.1 0.0
Depth from surface (m)
Footing south
Footing north
0.55
0.92
1.83
0 200 400 600 800 1000 1200 1400 1600
Time (s)
(e)
Subsrface settlement (m)
0.5 0.4 0.3 0.2 0.1 0.0
Initial depth of 0.46 m
Distance from footing center (m)
0.10
0.15
0.45
0.75
0 200 400 600 800 1000 1200 1400 1600
Time (s)

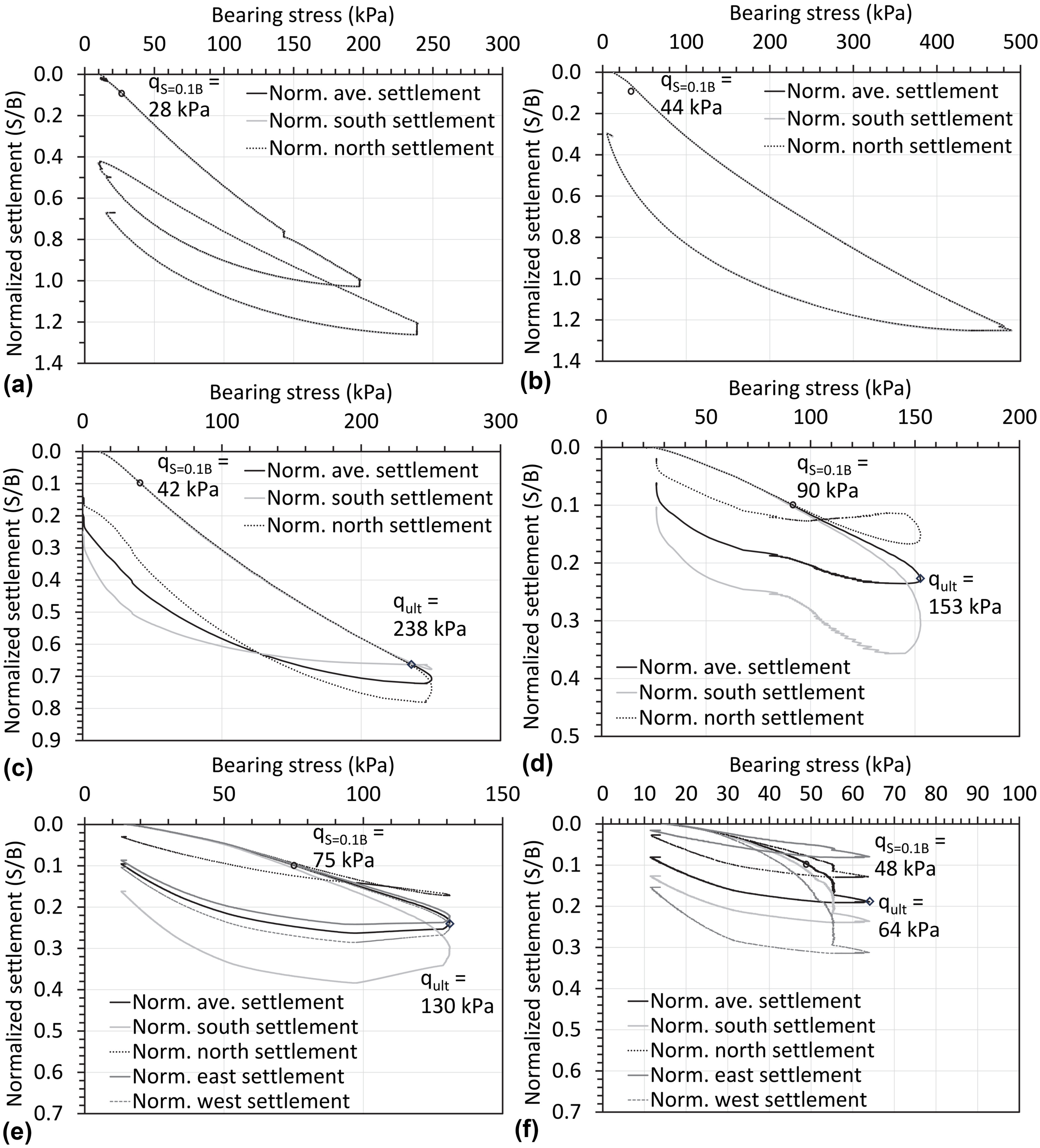
(a)
Bearing stress (kPa)
0 50 100 150 200 250 300
Normalized settlement (S/B)
0.0 0.2 0.4 0.6 0.8 1.0 1.2 1.4
$q_{S=0.1B}$ = 28 kPa
Norm. ave. settlement
Norm. south settlement
Norm. north settlement
(b)
Bearing stress (kPa)
0 100 200 300 400 500
$q_{S=0.1B}$ = 44 kPa
(c)
Bearing stress (kPa)
0 100 200 300
0.0 0.1 0.2 0.3 0.4 0.5 0.6 0.7 0.8 0.9
$q_{S=0.1B}$ = 42 kPa
q_{ult} = 238 kPa
(d)
Bearing stress (kPa)
0 50 100 150 200
0.0 0.1 0.2 0.3 0.4 0.5
$q_{S=0.1B}$ = 90 kPa
q_{ult} = 153 kPa
(e)
Bearing stress (kPa)
0 50 100 150
0.0 0.1 0.2 0.3 0.4 0.5 0.6 0.7
$q_{S=0.1B}$ = 75 kPa
q_{ult} = 130 kPa
Norm. east settlement
Norm. west settlement
(f)
Bearing stress (kPa)
0 10 20 30 40 50 60 70 80 90 100
$q_{S=0.1B}$ = 48 kPa
q_{ult} = 64 kPa

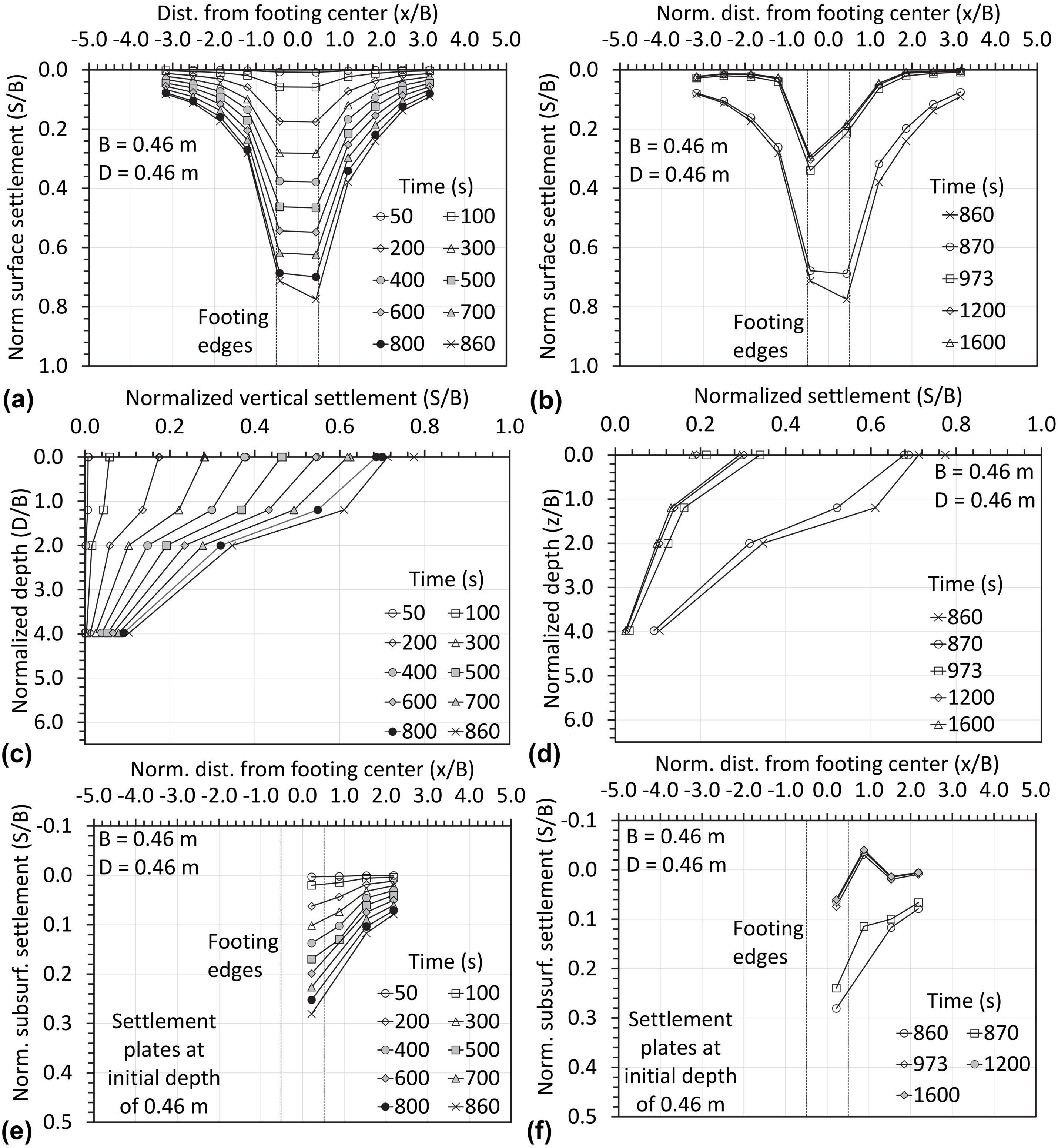

Dist. from footing center (x/B)
Norm surface settlement (S/B)
B = 0.46 m
D = 0.46 m
Time (s)
50 100 200 300 400 500 600 700 800 860
Footing edges
(a)
Norm. dist. from footing center (x/B)
Time (s)
860 870 973 1200 1600
(b)
Normalized vertical settlement (S/B)
Normalized depth (D/B)
(c)
Normalized settlement (S/B)
Normalized depth (z/B)
(d)
Norm. subsurf. settlement (S/B)
Settlement plates at initial depth of 0.46 m
(e)
(f)

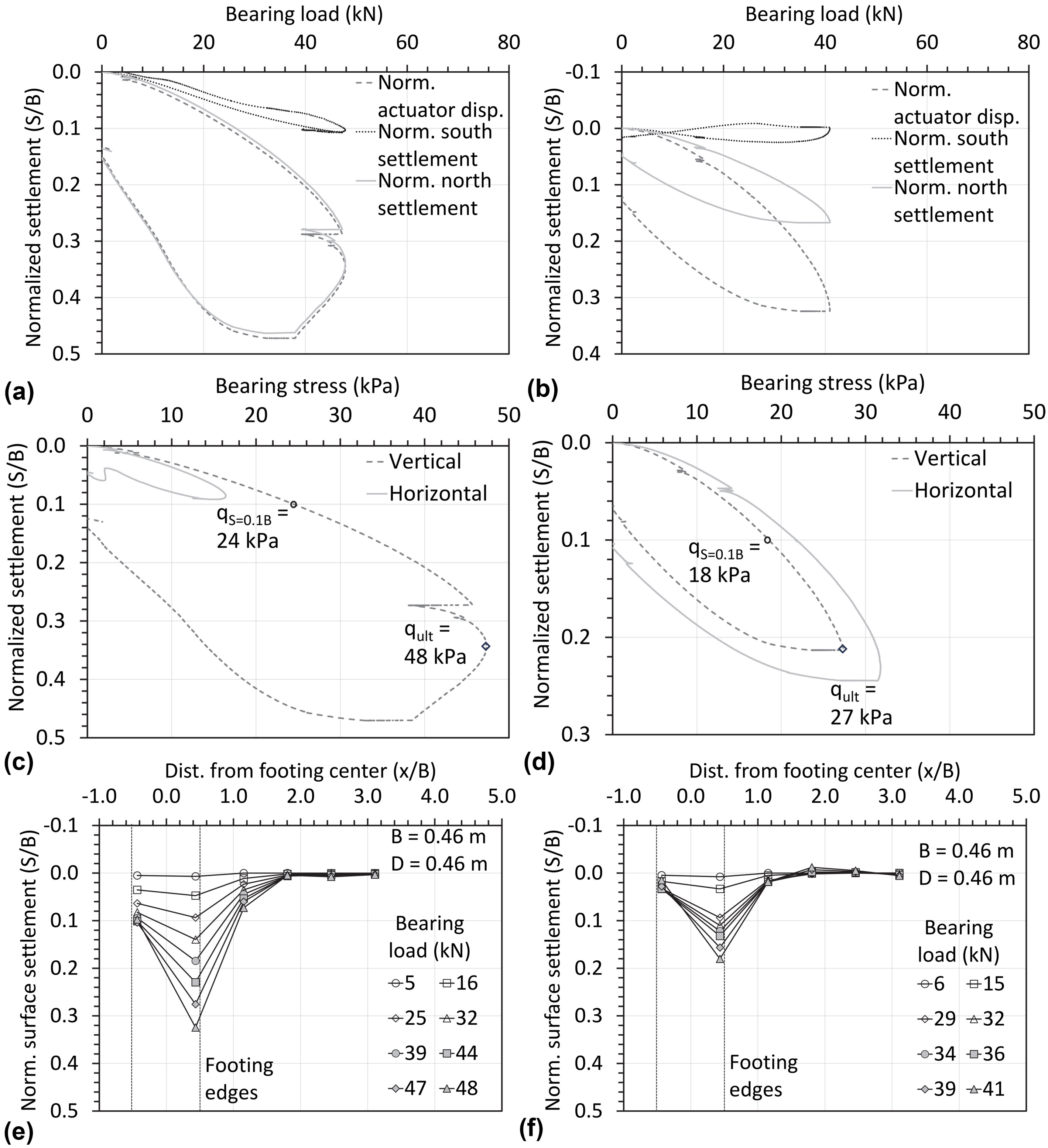

Bearing load (kN)
Normalized settlement (S/B)
Norm. actuator disp.
Norm. south settlement
Norm. north settlement
(a)
(b)
Bearing stress (kPa)
Vertical
Horizontal
q_S=0.1B = 24 kPa
q_ult = 48 kPa
q_S=0.1B = 18 kPa
q_ult = 27 kPa
(c)
(d)
Dist. from footing center (x/B)
Norm. surface settlement (S/B)
B = 0.46 m
D = 0.46 m
Bearing load (kN)
5 16 25 32 39 44 47 48
6 15 29 32 34 36 39 41
Footing edges
(e)
(f)

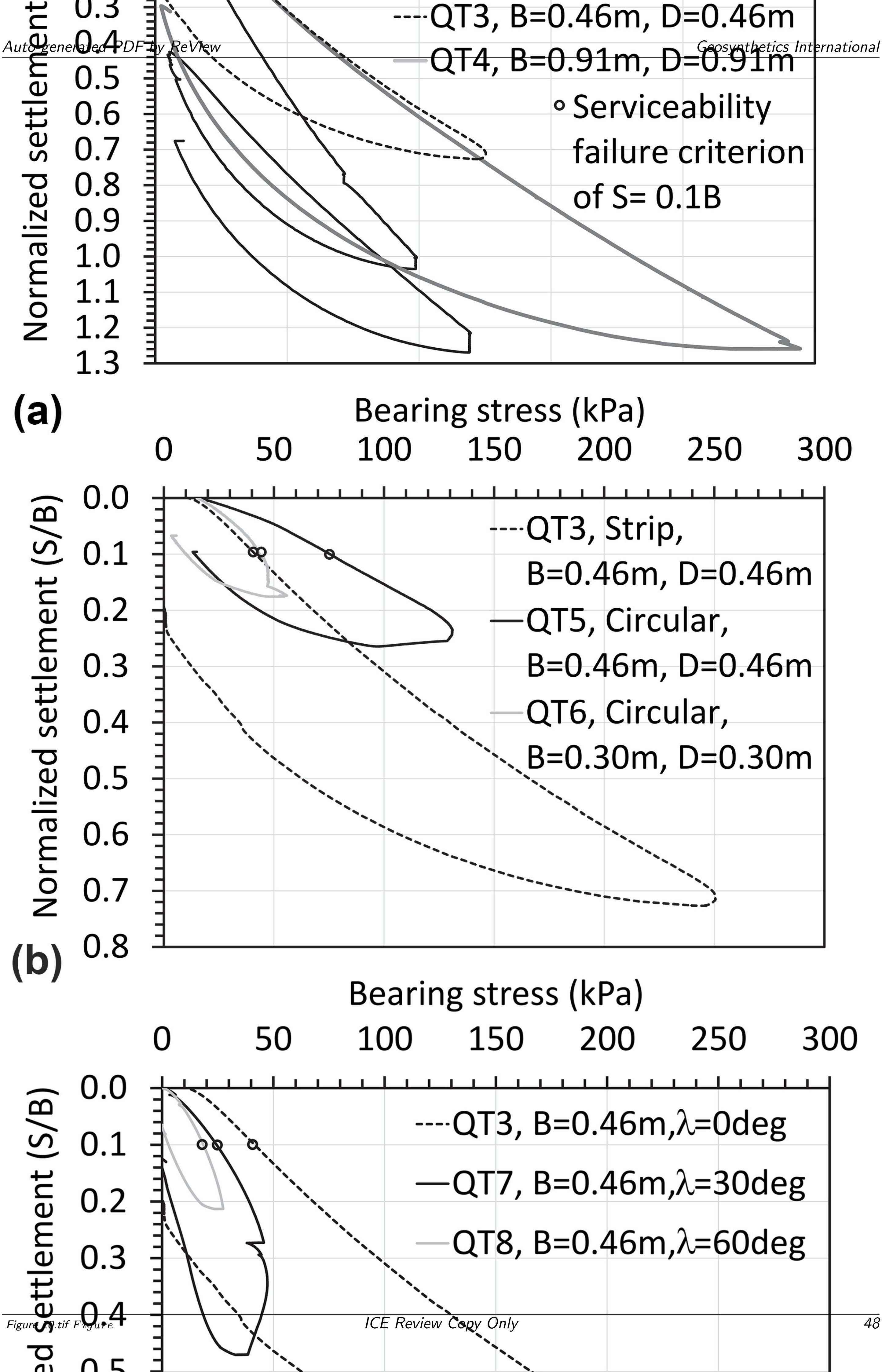

Normalized settlement
0.3
0.4
0.5
0.6
0.7
0.8
0.9
1.0
1.1
1.2
1.3
QT3, B=0.46m, D=0.46m
QT4, B=0.91m, D=0.91m
Serviceability failure criterion of S= 0.1B
(a)
Bearing stress (kPa)
0
50
100
150
200
250
300
Normalized settlement (S/B)
0.0
0.1
0.2
0.3
0.4
0.5
0.6
0.7
0.8
QT3, Strip, B=0.46m, D=0.46m
QT5, Circular, B=0.46m, D=0.46m
QT6, Circular, B=0.30m, D=0.30m
(b)
Bearing stress (kPa)
0
50
100
150
200
250
300
ed settlement (S/B)
0.0
0.1
0.2
0.3
0.4
0.5
QT3, B=0.46m,λ=0deg
QT7, B=0.46m,λ=30deg
QT8, B=0.46m,λ=60deg

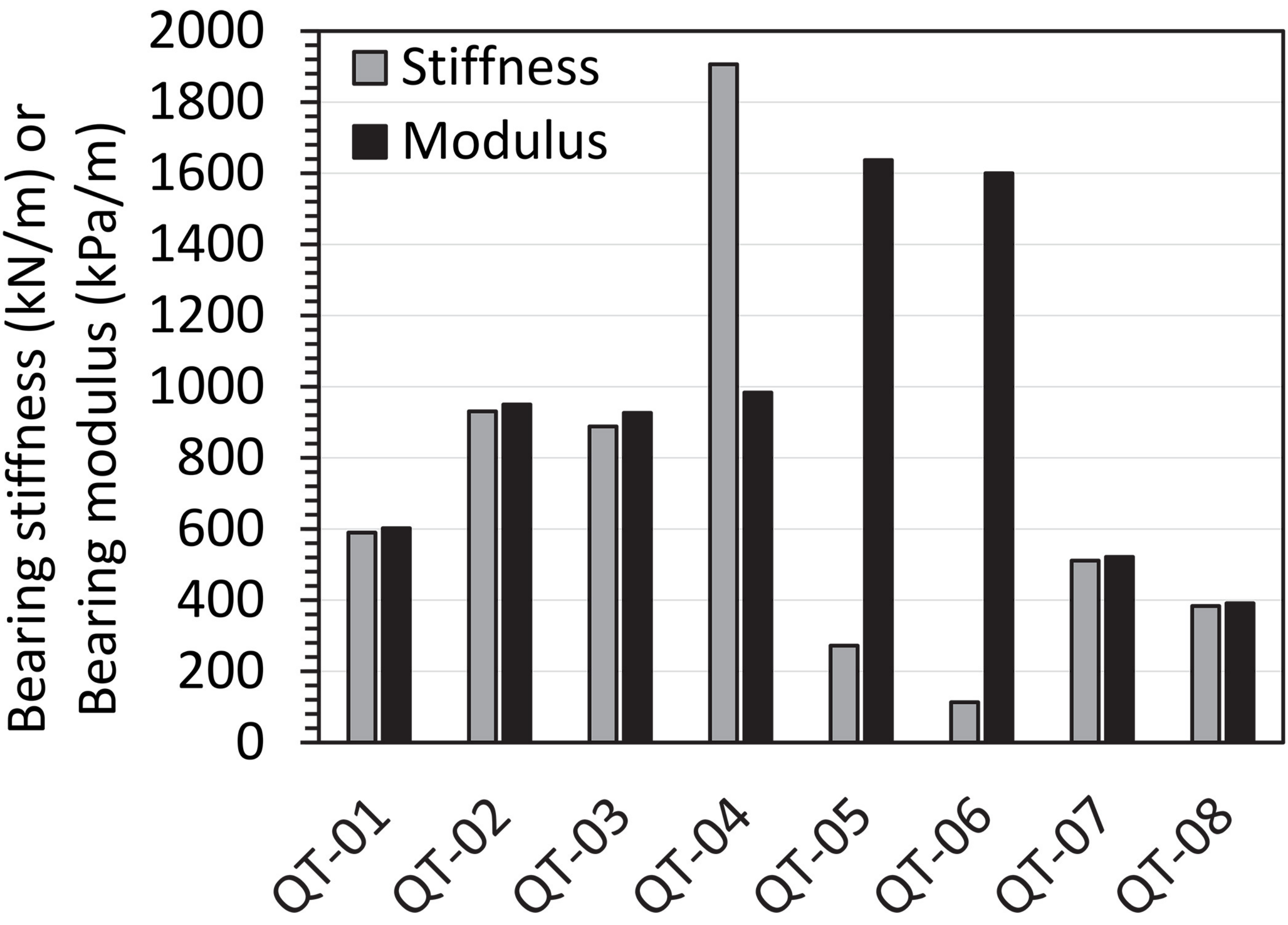
Bearing stiffness (kN/m) or
Bearing modulus (kPa/m)
2000
1800
1600
1400
1200
1000
800
600
400
200
0
Stiffness
Modulus
QT-01
QT-02
QT-03
QT-04
QT-05
QT-06
QT-07
QT-08

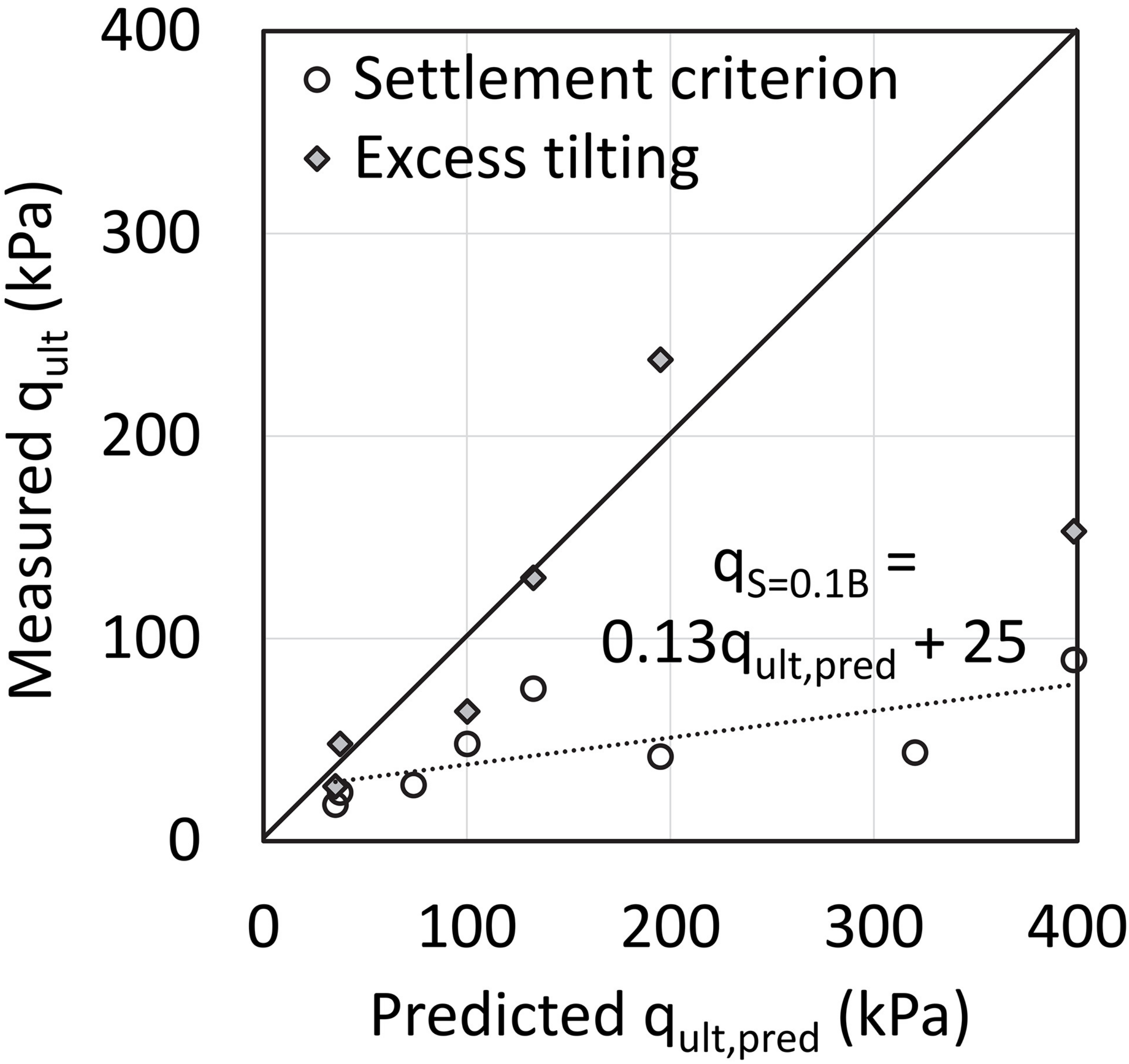
400
300
200
100
0
0
100
200
300
400
Settlement criterion
Excess tilting
$q_{S=0.1B}$ =
$0.13q_{ult,pred}$ + 25
Measured q_{ult} (kPa)
Predicted $q_{ult,pred}$ (kPa)

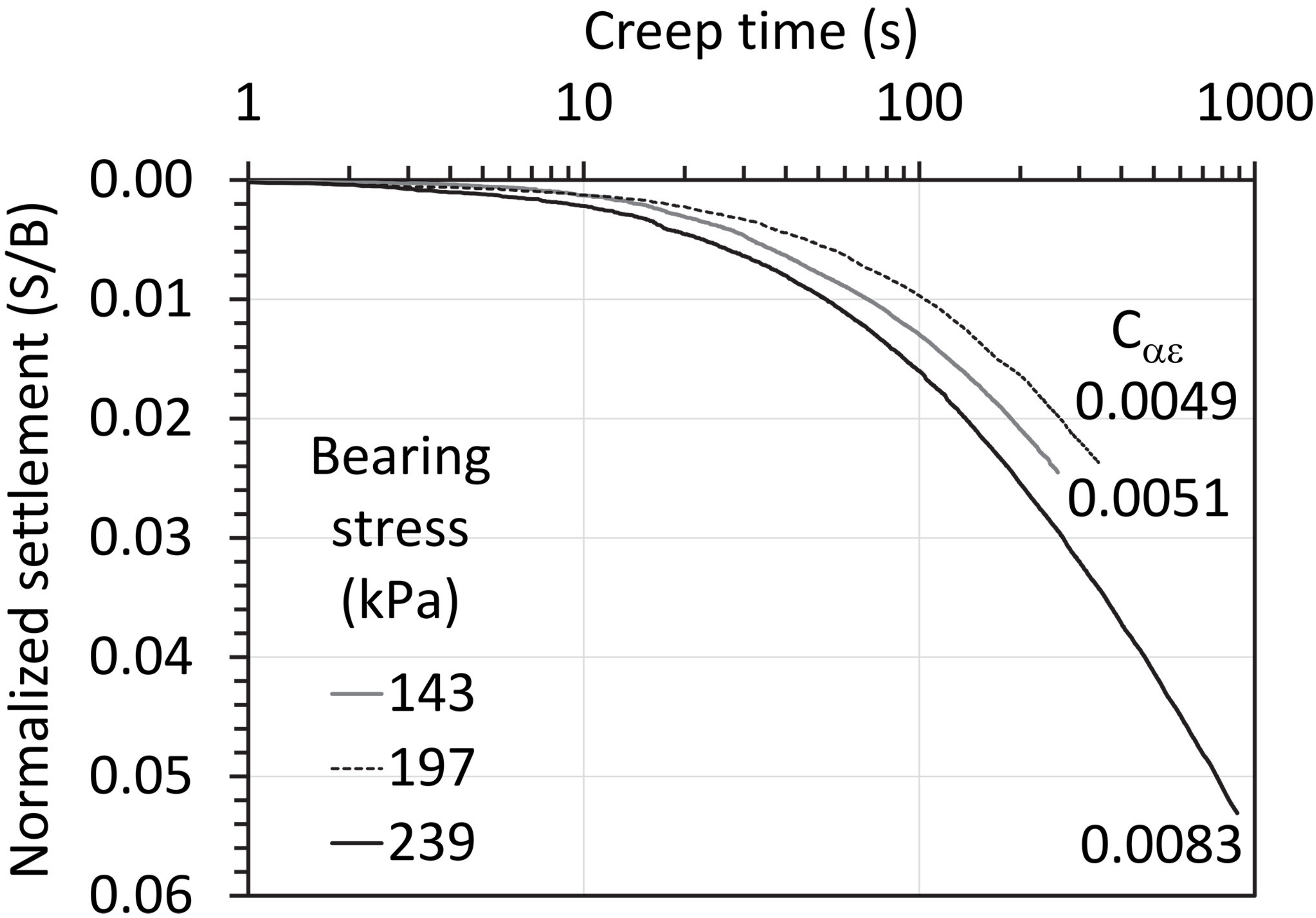
Creep time (s)
1
10
100
1000
Normalized settlement (S/B)
0.00
0.01
0.02
0.03
0.04
0.05
0.06
Bearing stress (kPa)
143
197
239
$C_{\alpha\varepsilon}$
0.0049
0.0051
0.0083